TD

Modelling Self-Organization on Electrodes of DC Glow Discharges

DOCTORAL THESIS

Matthew Simon Bieniek
DOCTORATE IN PHYSICS

UNIVERSIDADE da MADEIRA
A Nossa Universidade
www.uma.pt

February | 2018

Dedicated to Dina Moldovan

Acknowledgements

I thank supervisors for the contribution they have made to my academic, professional, and personal development. Also for inviting me into the environment they have helped to carve out in Madeira Island, where great science can be done, and new scientists can be trained.

I acknowledge Diego Santos for his efforts and talents in modelling that contributed to the work on identifying bifurcations.

I thank Helena Kaufman for her compnay during lunch, and for helping me to write the abstract for this thesis in Portuguese.

Also, I wish to thank my other colleagues for pleasant interactions and stimulating discussion.

Preamble

The work leading to this thesis was performed within activities of:

- FCT - Fundacão para a Ciência e a Tecnologia of Portugal through the project Pest-OE/UID/FIS/50010/2013.

Most of the results presented in this thesis are published in the following articles:

- M. S. Bieniek, P. G. C. Almeida, and M. S. Benilov, Modelling cathode spots in glow discharges in the cathode boundary layer geometry (2016), J. Phys. D: Appl. Phys. No. 49 105201
- M. S. Bieniek, D. Santos, P. G. C. Almeida, and M. S. Benilov, Bifurcations in the theory of current transfer to cathodes of dc discharges and observations of transitions between different modes

  Submitted in Feb 2018 to Phys. Plasmas
- M. S. Bieniek, P. G. C. Almeida, and M. S. Benilov, Self-consistent modelling of self-organized patterns of spots on anodes of DC glow discharges

  Submitted in Feb 2018 to Plasma Sources Sci. Technol

Results presented in this thesis were reported at the following conferences:

- M. S. Bieniek, P. G. C. Almeida, and M. S. Benilov, Modelling anode spots of DC glow discharges, in Proc. XXXIII ICPIG (9-14 July 2017, Estoril, Portugal)
- M. S. Bieniek, P. G. C. Almeida, and M. S. Benilov, Modelling cathode spots in glow discharges in the cathode boundary layer geometry with COMSOL Multiphysics , in Proc. XXXII (26-31 July 2015, Iasi, Romania)

Resumo

O trabalho apresentado nesta dissertação refere-se à modelação de padrões de auto-organização de densidade de corrente em elétrodos de descargas DC luminescentes.

Padrões de manchas anódicas foram modelados de forma auto-consistente pela primeira vez e os fenómenos nas manchas foram investigados. As soluções que descrevem as manchas foram encontradas num intervalo de correntes com múltiplas soluções. Foi descoberta uma inversão da densidade de corrente local do ânodo no centro de cada uma das manchas, isto é, mini-cátodos são formados dentro das manchas; poder-se-ia dizer, as manchas do ânodo funcionam como uma descarga luminescente unipolar. As soluções não se enquadram no padrão convencional de auto-organização em sistemas dissipativos não-lineares biestáveis; por exemplo, as transições de um modo para outro não se realizam através de bifurcações.

Padrões auto-organizados de manchas catódicas em descargas luminescentes foram modelados na camada de plasma junto ao cátodo, numa geometria igual à utilizada na maioria das experiências descritas na literatura. O efeito da geometria da câmara de descarga nas manchas foi investigado. Os padrões de manchas modelados são idênticos aos observados nas experiências e similares aos calculados na configuração de elétrodos planos em paralelo.

Uma tentativa foi feita para modelar quantitativamente a descarga DC luminescente com manchas catódicas. Uma descrição detalhada desta modelação, a mais precisa deste fenómeno até à data, é apresentada. Em geral, os padrões calculados são semelhantes aos observados nas experiências, mas as CVC são qualitativamente diferentes.

Cenários de transições entre modos com diferentes padrões de manchas em elétrodos de descargas DC luminescentes e em cátodos de descargas de arco são investigados. No caso de transições entre padrões em cátodos de descargas DC luminescentes, foram encontradas as transições observadas nas experiências que podem estar diretamente relacionados a bifurcações de soluções estacionárias, e as bifurcações correspondentes foram modeladas. Os padrões encontrados na modelação numérica estão em conformidade com os observados no decurso das transições nas experiências. No caso dos cátodos de descargas de arco, mostra-se que qualquer transição entre diferentes modos de transferência de corrente está relacionada a uma bifurcação de soluções estacionárias.

Palavras chave: Interacção plasma-cátodo, Auto-organização, Descargas luminescentes, Manchas no ânodo, Cátodos termiónicos, Manchas catódicas

Abstract

In this work self-organized patterns of current density on electrodes of dc glow discharges were modelled.

Patterns of anodic spots were modelled self-consistently for the first time and their physics was investigated. The solutions describing the spots were found to exist in a region of current with multiple solutions. A reversal of the local anode current density in the middle of each of the spots was discovered, i.e. mini-cathodes are formed inside the spots or, as one could say, the anode spots operate as a unipolar glow discharge. The solutions do not fit into the conventional pattern of self-organization in bistable nonlinear dissipative systems e.g. the modes are not joined by bifurcations.

Self-organized patterns of cathodic spots in glow discharges were computed in the cathode boundary layer geometry, which is the one employed in most of the experiments reported in the literature. The effect that the geometry of the vessel has on the spots was investigated. The computed spot patterns are the same as the ones observed in the experiment and similar to the ones computed in the parallel plane electrode configuration.

An unsuccessful attempt was made to quantitatively model DC glow discharge with cathodic spots, an account of this, the most accurate modelling of the phenomenon yet performed, is given. In general, the computed patterns are observed in the experiment but the CVC are qualitatively different.

Scenarios of transitions between modes with different patterns of spots on electrodes of dc glow discharges and cathodes of arc discharges are investigated. In the case of transitions between patterns on dc glow cathodes, those transitions reported in the experiments that may be directly related to bifurcations of steady-state solutions are found and the corresponding bifurcations are computed. Patterns found in the numerical modelling conform to those observed in the course of the transitions in the experiment. In the case of cathodes of arc discharges, it is shown that any transition between different modes of current transfer is related to a bifurcation of steady-state solutions.

Keywords: Plasma-electrode interaction, Self-organization, Glow discharges, Cathodic spots, Anodic spots

Contents

List of Figures

Chapter 1

Introduction

1.1 Direct current glow discharge

In 1838 Michael Faraday produced the first report of a direct current (DC) glow discharge [1]. Faraday, who used a voltaic pile as a power source, passed current through different gases, at various pressures, via electrodes in a glass bell jar. At low pressures, he observed a phosphorescent continuous glow around one of his electrodes, which he described as "exceedingly beautiful". The main features of a DC glow discharge can be read about in the textbook by Raizer [2]. The discharge has been significant in both fundamental plasma science and in applied plasma science. DC glow discharges have been used in spectroscopy [3], allowing research on the elements of materials in the gas, liquid, and solid state; laser technology [4], with laser gain medium being electrically pumped by DC glow discharge; surface property modification [5], that atmospheric pressure glow discharge may adapt the wetting properties of a surface; cancer inhibition research [6], glows with liquid anodes have been demonstrated to suppress the activity of at least two types of cancer cell, *in vitro*; sources of ultraviolet radiation [7], that DC glow microdischarges, when configured to yield high energy electrons in a high pressure gas, result in excimer production; to name just a few examples of DC glow discharge being utilized in science.

1.1.1 Modelling and theory during the 20th century

A well-known one-dimensional description of the cathode fall was formulated in 1934 by von Engel and Steenbeck [2]. The description reveals a U-shaped current density voltage characteristic (CDVC). However, the transition from the Townsend discharge to the abnormal discharge, as revealed by the von Engel and Steenbeck solution, is particularly different to what is observed in experiments. Instead of the normal discharge observed in the experiments, the solution by von Engel and Steenbeck has a

one-dimensional distribution of charged particles, and reveals a falling CDVC section. While von Engel comments that the causes of the differences are basically not understood [8], Steenbeck proposes arguments to describe the observed physics of the normal discharge on the basis that the axial electric field ought to be minimized [9] (the so-called 'Steenbeck's principle of minimum power', which became more widely accepted as it was reported that this principle is a corollary of the principle of minimum entropy production [10]). The rising section of the CDVC associated with the von Engel and Steenbeck solution corresponds with the abnormal discharge in a qualitatively accurate way.

Circa 1960, glow discharge modelling results started to be found with the aid of electronic computers [11, 12]. The authors aimed to solve the relevant, coupled, physical equations: in [12], equations of conservation of number density of electrons and ions (considering only drift fluxes), and Poisson's equation, were solved. An effective Townsend ionization coefficient was used (recombination was neglected). The results essentially duplicated von Engel and Steenbeck's solution. In particular, there was agreement, whereby under particular conditions[1], the CDVC was U-shaped.

In the 1980s, two-dimensional modelling of glow discharges started to emerge (e.g. [14–16]) which, based on similar underlying physics as the one-dimensional models, revealed the structure of the normal spot. In 1988 [17] Boeuf solved a two-dimensional model, and found the structure of the normal spot, the normal current density effect, and the current-voltage characteristic (CVC) plateau associated with the normal spot. The basic mechanisms of the model are drift and diffusion for the ions and the electrons, volume ionization, recombination, and secondary electron emission. The model yielded an accurate qualitative description of the transverse behavior of the transition from the abnormal mode to the normal model.

The aforementioned modelling used a fluid description of the plasma. This approach is based on the taking of moments of the Boltzmann equation (BE) (e.g. [18, 19]), for each of the species considered, coupled with the Poisson equation (or the relevant set of Maxwell's equations). For that sake of practicality, it is normally the case that the electron energy distribution function is assumed to be either Maxwellian or a two term spherical harmonic expansion with the second term accounting for an anisotropic perturbation [20]. The set of equations generated from the taking of the moments of the BE are closed, in the case of the electrons, typically at the level of either momentum, or energy. In the case of momentum, one typically employs the drift-diffusion approximation, with the transport and kinetic coefficients related to

[1] If a discharge, by way of its product of pressure and the distance of electrode separation, would have a breakdown voltage on the rising section of the Paschen curve, then it will have a U-shaped CVC (i.e. it will not be an obstructed discharge) [13].

space and time by functions (built using the solution to the BE) with the reduced electric field as their argument: the so-called local-field approximation (LFA). The LFA is suitable when the characteristic length of electron energy relaxation is small compared to a characteristic discharge length. When one includes in the set of equations to be solved an equation for electron energy, the transport and kinetic coefficients for the charged species may be related to space and time by a function (built using the solution to the BE) with the average of electron energy as the argument: the so-called local mean energy approximation. The latter approximation is more accurate and allows for the study effects such as striations [21].

Strictly speaking, one should only use the fluid-based approach to the modelling of a plasma when that plasma has an energy distribution function for the charged species that are Maxwellian (although, fluid approaches may perform 'better than they should', e.g. [22] p. 35). When a fluid-based approach is not appropriate, one may employ a kinetic-based approach to modelling [23] e.g. when the species are in a strongly non-uniform field (as may be the case in the cathode fall [24]), and regions with few collisions. In general, the kinetic based approach requires a greater computational effort, but fewer a priori assumptions.

By the end of the 21st century, the main features of the discharge, e.g. those discussed in chapter 8 of [2], had been, quite faithfully, reproduced by computer models.

1.2 Self organization

The term self-organisation is used in various disparate academic disciplines. In social science [25], it is used in connection with phenomena such as city formation; in computer science [26], in connection with methods of utilizing idle system components; in biology [27], used in the context of morphogenesis, whereby identical cells may differentiate into, for example, an organism with eyes. Broadly, the term self organization is used to describe the spontaneous occurrence of order among multiple subunits, from a source other than the direct motivation of an external influence.

In this thesis, the term self-organisation is used to refer to the occurrence of dissipative structures. Prigogine coins the term 'dissipative structure' [28] in 1967, referring to structures, or patterns of structures, with a clear degree of spatial regularity, which form in conditions far from thermodynamic equilibrium, and are maintained by fluxes of matter and energy. The emergence of spatiotemporal structures (e.g. the Belousov–Zhabotinsky reaction [29]), are neglected in this thesis.

In section 1.2.1 the thermodynamics of self-organisation are commented on for the sake of historical and scientific context. In sections 1.2.2 and 1.2.3 the concepts are briefly introduced of stability, and bifurcations, respectively.

1.2.1 Thermodynamics of self organization

Prigogine's textbook [30] on self-organization introduces dissipative structures in the same way as in this section.

It is well known that the second law of thermodynamics prevents the spontaneous formation of order in isolated systems. Also, that in such systems there is a coupling between the degree of order in the system and its evolution, and ultimately its stability. In closed systems, whereby exchanges of heat with outside reservoirs are permitted, ordered structures may arise: Helmholtz free energy is minimized at thermodynamic equilibrium and for low temperatures the probability that a particle in the system is at a state of a low energy level (by Boltzmann's ordering principle [31]) is high, hence solid crystals or phase transitions occur. At moderate temperatures (e.g. the temperature of animal cells), however, the probability of the formation low entropy structures, via the former ordering principle, is prohibitively small, and yet, order in cells exist. Apparently a different source of order is also available to nature.

A class of thermodynamic system termed 'open' was studied at the de Donder school in Brussels (see e.g. books by von Bertalanffy [32] and E. Schrodinger [33] on the physics of life), i.e. a thermodynamic system was studied that takes into account exchanges of matter and heat with its surroundings. Prigogine in 1945, working from the school, makes the contribution of extending the second law of thermodynamics to such open systems. Entropy change is considered in a time interval, and decomposed into two contributions: entropy flux due to exchanges with the environment, and entropy production due to irreversible processes inside the system. The change in entropy in time can therefore be negative, as exchanges of negative entropy from outside system may be dominant (change in entropy would regularly be seen as being only positive, if one only considered isolated systems). Thus in principle, ordered structures may arise in open systems as long they are being maintained by fluxes of matter and energy with 'negative entropy'. Such structures are termed 'dissipative structures'. Many apparent examples of such structures are listed in [34]. An early example of which, observed by Lehmann in 1902 [35], is a localized solitary luminous spot found on an anode of a DC glow discharge.

Prigogine's textbook points to unfinished thinking on a criterion based on thermodynamic state functions (e.g. entropy, entropy production), for the onset of dissipative structures. A comment is made that such structures may coincide with a minimum of entropy production. Contemporary academics are still debating the possibility of finding such a general thermodynamic criterion [36].

The general criterion of Steenbeck's principle of minimum power in gas discharge physics has been found to be not without problems. An example of such a problem

follows. Within the framework of a model of nonlinear surface heating of a cathode of an arc discharge, a computed solution associated with the lowest discharge voltage was selected, from among several other solutions existing for the same discharge current, as the one that is stable [37] based on Steenbeck's principle of minimum power. However, numerical results presented in [38] and the analytical theory [39] indicate that the low-voltage branch is unstable, and the high-voltage branch is stable. Further, even if it was found that the principle of minimum entropy production was valid for gas discharges, Steenbeck's principle of minimum power is shown [40] to not be a corollary of the principle of minimum entropy production. Hence, an understanding of the general theory of stability is important in situations with multiple solutions.

1.2.2 An introduction to stability

The literature on stability is well developed (see e.g. the textbook [41]). The concept and some common approaches to studying stability are briefly introduced in this section.

A system of differential equations governing the evolution of variables in a space, such as phase space, may be constructed using first principles such as classical physics and potential fields. A solution to those equations is said to be stable if the time evolution of an initial state plus a perturbation will remain close to the initial state at all subsequent moments. Otherwise, the solution is unstable. One may describe a solution as locally stable, globally stable, or stable against a particular perturbation. A solution is globally stable if any perturbation on an initial state would result in an evolution of the solution that would have it return to the initial state. A solution is locally stable, or metastable, if any small perturbation on the solution would result in an evolution of the solution that would have the solution return to the initial state.

One may employ different approaches when studying stability e.g. using the Lyapunov stability criterion [30]: one constructs a function whose rate of change determines if an initial state is 'asymptotically stable' (i.e. if it is stable against *any* small perturbation). It is not always straightforward, and may even be impossible, to identify a suitable function in a given situation. Another approach is to use linear stability theory [42]: an initial state under investigation and a small perturbation with an exponential time dependence is substituted into the system of equations and boundary conditions. The problem is linearized with respect to the perturbation, resulting in an eigenvalue problem whose spectrum describes the mode of development, or damping, of the perturbation. With the eigenvalues being the growth increment of the perturbations. If real parts of all eigenvalues are negative, the state is stable; if at least one eigenvalue has a positive real part, the state is unstable.

1.2.3 An introduction to bifurcations

A concise summary of the information from bifurcation theory relevant to this thesis can be found in the Appendix of [43]; a more detailed discussion of the theory can be found in, e.g., the review [44]. A brief introduction to bifurcations follows.

A bifurcation is a splitting of a solution occurring when one varies a system control parameter past a certain critical point (the bifurcation point). The splitting corresponds with a qualitative or topological change to the solution(s) past the bifurcation point. An example is the pitchfork bifurcation: consider a two-dimensional (axially symmetric) solution describing, for instance, the spatial distribution of the number density of some particles in a three-dimensional space, that varies with a control parameter p. At $p = p_0$ there exists a bifurcation point, before and after the bifurcation point the stability of the solution changes[2] (for definiteness, the solution is stable for $p > p_0$ and unstable for $p < p_0$). At p_0 a three-dimensional solution also exists, that branches off away from the two-dimensional solution. If the three-dimensional solution branches off into the range $p < p_0$, where the two-dimensional solution is unstable, then the pitchfork bifurcation is supercritical. One would observe, as one varies from high to low p, along the solutions that are stable, a smooth transition from the two-dimensional distribution of the number density to a three-dimensional distribution. The effect of symmetry breaking leads to an ordering of the solution (e.g. a bifurcation point on an axially symmetric two-dimensional solution may lead to a three-dimensional solution with azimuthal periodicity; from e.g. a torus like distribution to a distribution in the form of a ring of equidistant spheres).

1.3 Self organization of spots on electrodes of glow discharges

1.3.1 Observations of spots on cathodes of glow discharges

The earliest examples of observations of luminous spots of current density on cathodes of glow discharges were of the solitary normal spot e.g. as in Figure 16 of [45].

In 2004, during a study of DC glow microdischarges as sources of excimer emission [46], organized patterns of luminous spots of current density on the cathode, as in Figure 1.1, were observed. During the last decade many accounts were made of such spots [7, 46–54]. The patterns have been observed for different gases [55] (infact, the experiments on self-organization on cathodes of DC glow microdischarges in gases other than xenon were motivated by the prediction, generated from modelling

[2] In the context of linear stability analysis, a bifurcation coincides with the switching of the sign of an eigenvalue.

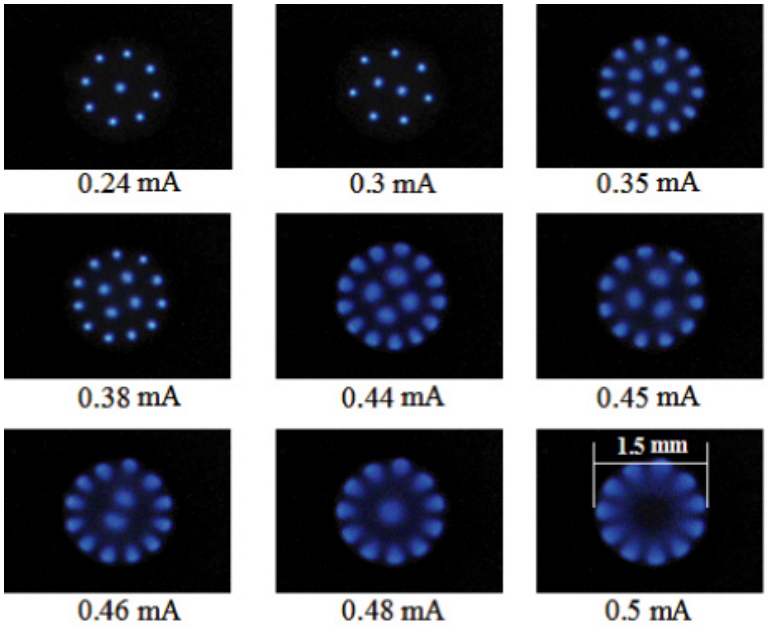

Figure 1.1: Patterns of lumous spots of current density on a cathode of a DC glow microdischarge, for different values of discharge current. Xenon under a pressure of 75 torr. Reprinted from [46].

results, that the patterns can occur in alternative plasma-producing gases). In terms of discharge geometry, the vast majority of the experiments have been performed in the so-called cathode boundary layer configuration, a device comprising a flat cathode and a ring-shaped anode, separated by a dielectric (cf., e.g., Figure 1 of [54]). Note that the modelling had only been performed for discharges with parallel-plane electrodes [42, 43, 53, 56–58]. Experiments that were performed in the parallel-plane electrode configuration show [49] self-organized patterns that are similar to the ones found in the cathode boundary layer configuration.

Spot patterns on cathodes of DC glow discharges have so far only been directly observed in microdischarges. There is currently no explanation why the patterns have not been observed in larger devices. Indications that the patterns also occur in larger atmospheric pressure glow discharges exist in the form of unexplained erosion patterns on cathodes [59], and observations of ring and cog-like structures [60].

1.3.2 Theory and modelling of cathode spots

As discussed in section 1.1.1, the CDVC revealed by the analysis of von Engel and Steenbeck, and the CDVC computed in one-dimensional simulations [11, 12], are U-shaped. However, if one includes in consideration the discharge solution describing 'no'

discharge (the trivial solution), of 0 A from 0 V to the breakdown voltage, then instead of a U-shaped CDVC one finds an N-shaped CDVC. The left-hand branch belonging to the stable unlit discharge, the right hand branch belonging to the stable abnormal discharge, and the central branch belonging to the unstable region with a negative differential resistance. That the system is N-shaped and bistable is an indication that phase coexistence will manifest [61]. The falling section of the 'N' is unstable and, in order for a discharge to be found in an experiment at those values of current, a stable solution ought to exist in that region of current too. One may attempt to employ a Maxwell construction[3] to find a stable branch [62]. The new stable branch would correspond with a solution describing a coexistence of the stable states on either side of the N-shaped system (see e.g. Figure 5. of [63]).

In 1988 Benilov [64] proves that within a basic model used to describe a glow discharge (one similar to [12]) there exists multiple solutions in the same range of currents: a one dimensional solution, and multidimensional solutions bifurcating from the one dimensional solution near the beginning and end of the CVC region with negative differential resistance. Benilov proposes that the multidimensional solution(s) may describe the behavior of the normal discharge. In 2010 Almeida proves this hypothesis [56] by means of numerical simulation: a two-dimensional solution is computed that indeed reproduces the behavior of the normal mode (a solution similar to the one found by Boeuf [24]) which bifurcates from the one-dimensional solution: CVC in Figure 1.2.

The description of the normal discharge as a coexistence of the abnormal discharge and the unlit discharge is very convincing. It (apparently, alone) explains the normal current density effect: for a decreasing current, less plasma is in the stable state of the abnormal discharge (the abnormal discharge at a particular voltage), and with the system being bistable, the plasma converts to, the only other stable configuration, the unlit discharge.

In 2011 Almeida [42], using the theoretical description of multiple solutions developed to describe the normal mode, computed three-dimensional patterns of spots on the cathodes of microdischarges (see Figure 1.3).

Modelling has since provided a wealth of modes and the comparison between the spots found in these modes and the spots observed in the experiment (those from section 1.3.1) is convincing.

[3] A classical example of a Maxwell's construction is performed on van der Waals equation of state at low temperatures. The original N-shaped isotherm has its falling section (on the 'N') supplemented with a thermodynamically stable horizontal section.

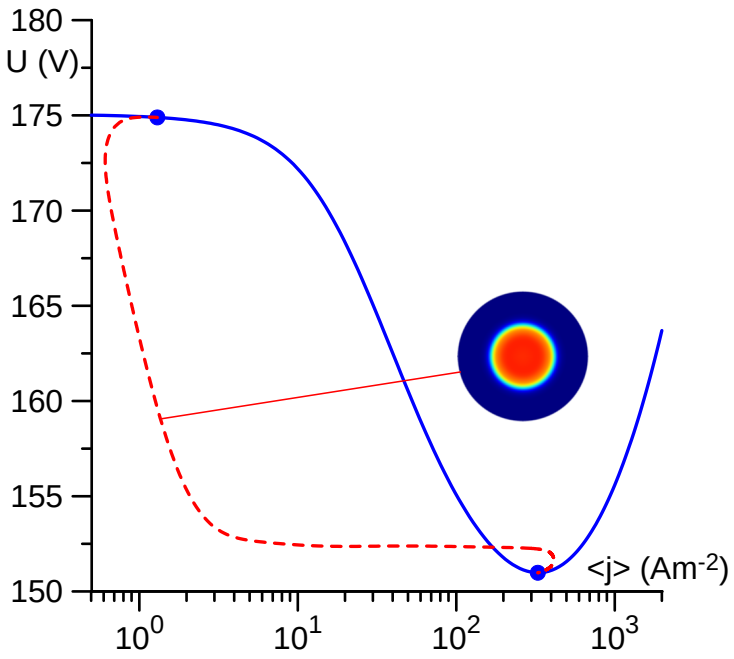

Figure 1.2: Computed CVC of DC glow discharge. Solid line: 1D mode. Dashed line: 2D modes. Circles: bifurcation points. Xe plasma. Pressure of 30 Torr. Adapted from [56].

1.3.3 Observations of spots on anodes of glow discharges

Luminous spots on anodes of DC glow discharges have been observed for over a century now e.g., [35, 65–71]. The spots have been observed in a wide range of pressures [65, 71], and in different gases [66]. At low pressures, a connection has been observed with the various types of double layer structures (e.g.[72–77]). Single spots have been studied in some depth and are being utilized as ion sources (which can produce a stable and high-current ion beam) [78].

1.3.4 Theory and modelling of anode spots

The current theoretical framework for the patterns of luminous spots of current density on anodes is not well developed. For instance, no self-consistent modelling has been performed (modelling had been performed that revealed current density structures e.g. [79], but these, apparently, treated the column as a cathode). A detailed description of the spots is absent.

A theoretical analysis, and experimental investigation, of the anode layer region is performed in [80] which indicates that instabilities found in the regions' so-called subnormal regime are a precursor for the formation of anode spots. In relation to

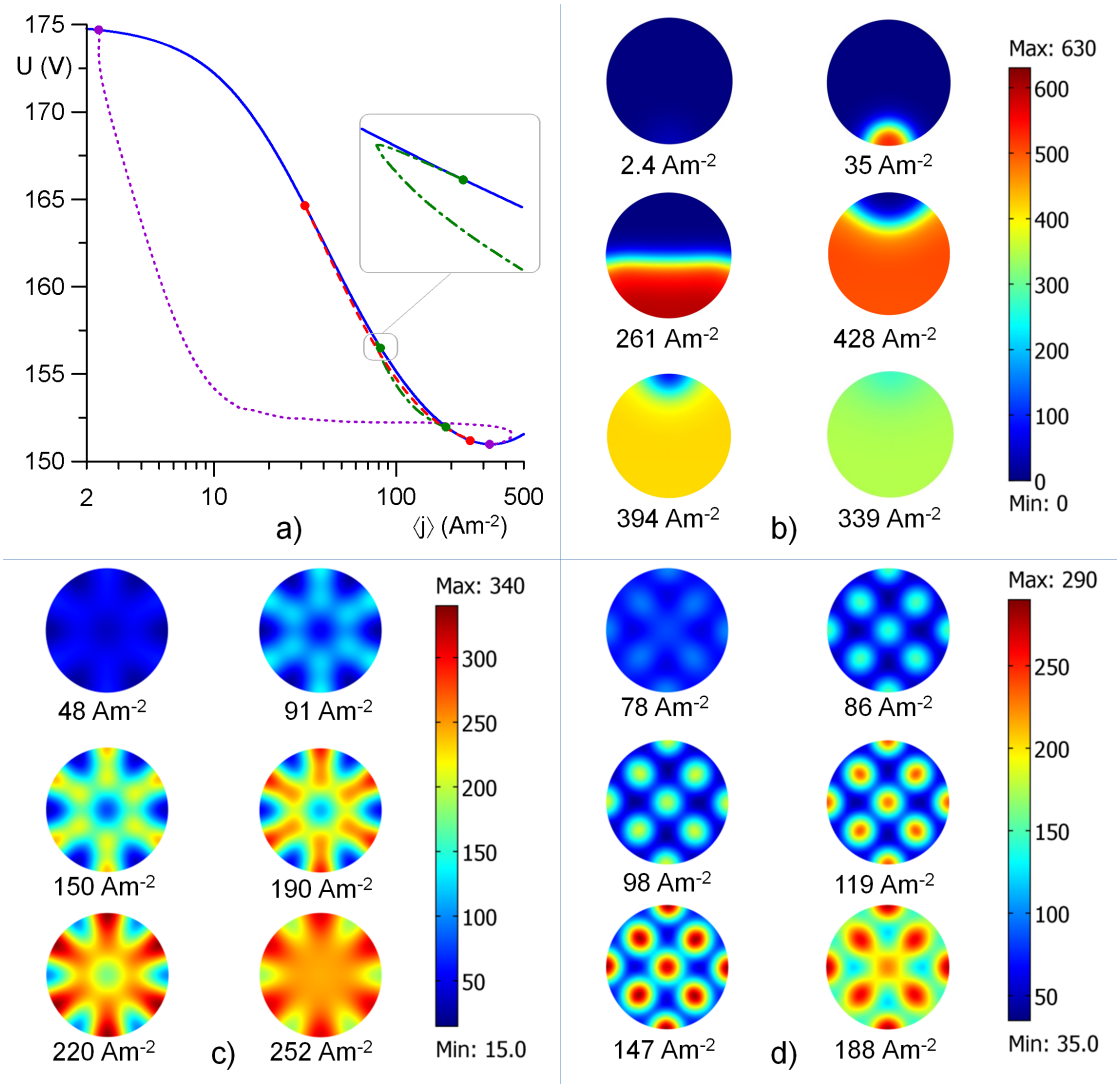

Figure 1.3: a) CVC of 1D and 3D modes. b-d) distributions of current density over the cathode surface. Solid line: 1-D mode. Dotted line: 1st (in order of decreasing current) 3D mode. Dashed line: 8th 3D mode. Dashed-dotted line: 12th 3D modes. Circles: Bifurcation points. (b).(d) Distributions of current density for (b) 1st 3D mode (c) 8th 3D mode (d) 12th 3D mode. Reprinted from [42].

double layers, a theoretical analysis by [76] also indicates precursors for the onset of spots (a positive anode bias above a threshold value).

Patterns of spots have been calculated by means of a phenomenological theory, based on the general trends of self-organization by [69].

1.4 This work

The questions that will be addressed in this thesis are discussed in this section.

Can the well developed theoretical interpretation of cathodic spots be applied to the spots found on anodes of DC glow discharges? What is the behavior of the anode spots? In chapter 2 a report is given of self-consistent modelling of patterns of anodic spots, the physics of the spots is investigated. The solutions describing the anode spots are compared to the cathode spots and the conventional pattern of self-organization in bistable nonlinear dissipative systems.

To what extent does the vessel geometry effect the patterns of the spots found on cathodes of DC glow microdischarges? In the chapter 3 a report is given of modelling of self-organized patterns of cathodic spots in the cathode boundary layer geometry, which is the one employed in most of the experiments reported in the literature. The modelling is compared to prior modelling done in the plane parallel geometry and to the spots observed in the experiment.

Can modelling of cathode spots on glow microdischarges be quantitatively accurate? In the chapter 4 a report of 3D fluid modelling of the cathodic spots is performed for the experimental conditions, using the local mean energy approximation, an account of several plasma and gas species, and a fairly detailed account of their reactions. The modelling results are compared to the experimental accounts.

Can direct proof of bifurcations in DC gas discharges be found? In chapter 4 a report is given of an analysis of scenarios of transitions between modes with different patterns of spots on electrodes of DC glow discharges and cathodes of arc discharges. In the case of transitions between patterns on cathodes of DC glowdischarges, experimental reports are found that appear to be related to bifurcations of steady-state solutions, the corresponding bifurcations are computed.

Chapter 2

Anode spots

2.1 Introduction

For more than a century now beautiful patterns on anodes of DC glow discharges have been observed [35, 65–71]. The patterns are of significant theoretical interest in themselves, and also because of their connection with various types of double layer structures, which have been studied at low gas pressures [72, 73, 75–77]. The patterns are interesting also from the point of view of their technological applications. As examples, we note that single spots have been utilized as ion sources with a stable and high-current ion beam extraction [78], and recently it has been shown that self-organized patterns on liquid anodes of atmospheric pressure glow microdischarges can reveal a nontrivial cancer-inhibiting capability [81].

A theoretical analysis, and experimental investigation, of the anode layer region performed in [80] indicates that instabilities found in the regions' so-called subnormal regime are a precursor for the formation of anode spots. Also in [80], the influence that the spots have on the homogeneity of the plasma column is investigated. A theoretical analysis of anode spots in relation to double layers is given by [76], which predicts an onset of spots for a anode biases below a threshold value. Numerical simulations have been performed which revealed current density stripes on anodes [79], a circular spot [82], and a circular spot surrounded by a ring [82]. Patterns of spots have been calculated by means of a phenomenological approach based on the general trends of self-organization in [69].

Self-organized arrangements of spots and patterns on cathodes of DC arc and glow discharges have been understood and systematically described in terms of multiple steady-state solutions, which exist in conventional models of glow discharge over the same range of discharge current and describe modes associated with different cathode spots and cathode spot patterns; e.g., [83] and references therein. We hypothesize

that the same approach is applicable to spots and spot patterns on anodes of DC glow discharges. In other words, we postulate that spots and spot patterns on anodes of DC glow discharges can be described by a new class of solutions, that exist in conventional models of glow discharges, alongside the solution associated with the spotless mode of current transfer. In this work we prove this hypothesis. Two solutions, as examples, are computed over the same, wide, range of current. One solution describes an axially symmetric diffuse, or spotless, mode, and the other solution describes a three-dimensional mode with azimuthal periodicity comprising a self-organized pattern of 8 anode spots.

The outline of the chapter is as follows. The model is described in section 2.2. In section 2.3, results of the modelling are given and discussed. Conclusions are drawn in section 2.4.

2.2 The model

Consider a cylindrical DC glow discharge tube that is long enough that the effect of the electrodes become obviated in the column. In the column the density of charged species and electric field are independent of the axial coordinate. This invariance allows us to choose an asymptotically accurate set of boundary conditions on a domain that contains only the region from the anode to the column. The computation domain is adequate for an investigation of anode spots, or patterns of spots, appearing as a result of processes of plasma-anode interaction only.

The simplest model of a glow discharge is used, which is well-known but briefly summarized here for completeness. It comprises equations for conservation of electrons and a single ion species, the transport equations, written in the drift-diffusion approximation, and Poisson's equation:

$$\begin{aligned} \frac{\partial n_i}{\partial t} + \nabla \cdot \mathbf{J}_i &= n_e \, \alpha \, \mu_e \, E - \beta \, n_e \, n_i, \quad \mathbf{J}_i = -D_i \, \nabla n_i - n_i \, \mu_i \, \nabla \varphi, \\ \frac{\partial n_e}{\partial t} + \nabla \cdot \mathbf{J}_e &= n_e \, \alpha \, \mu_e \, E - \beta \, n_e \, n_i, \quad \mathbf{J}_e = -D_e \, \nabla n_e + n_e \, \mu_e \, \nabla \varphi, \\ \varepsilon_0 \, \nabla^2 \varphi &= -e \, (n_i - n_e) \, . \end{aligned} \tag{2.1}$$

Here n_i, n_e, $\mathbf{J}_i$, $\mathbf{J}_e$, D_i, D_e, μ_i, and μ_e are number densities, densities of transport fluxes, diffusion coefficients, and mobilities of the ions and electrons, respectively; α is Townsend's ionization coefficient; β is coefficient of dissociative recombination; φ is electrostatic potential, $E = |\nabla \varphi|$ is electric field strength; ε_0 is permittivity of free space; and e is elementary charge. The local-field approximation is employed, i.e.,

electron transport and kinetic coefficients are assumed to depend on the local electric field only.

Let us introduce cylindrical coordinates (r, ϕ, z) with the longitudinal axis in line with the axis of the discharge tube. The computation domain is a cylinder $\{0 \le r \le R\}$, $\{0 \le \phi \le 2\pi\}$,$\{0 \le z \le h\}$ where R is the tube radius and the boundary $z = h$ is positioned in the discharge column.

Standard boundary conditions are used for the lateral dielectric wall, $r = R$, describing absorption of ions and electrons, and electrical insulation:

$$J_{in} = \sqrt{\frac{8k_BT_i}{\pi m_i}}\frac{n_i}{4},\ J_{en}=\sqrt{\frac{8k_BT_e}{\pi m_e}}\frac{n_e}{2},\ J_{in} - J_{en} = 0. \tag{2.2}$$

Here subscript n represents the projection of the corresponding vector along n the normal directed outside the computation domain, k_B is Boltzmann's constant, T_i and T_e are ion and electron temperatures (known parameters), m_i and m_e are the ion and electron masses. When a time-dependent solver is used, the last condition in equation (2.2) is replaced by the following boundary condition

$$-\varepsilon_0\frac{\partial\varphi}{\partial n} = \rho_s,\ \frac{\partial\rho_s}{\partial t} = e\left(J_{in} - J_{en}\right), \tag{2.3}$$

which describes surface charge accumulation; here ε_0 is permittivity of free space and ρ_s is surface charge density. If a steady-state has been reached, these conditions are equivalent to the last condition in equation (2.2).

Boundary conditions at the anode surface ($z = 0$) are

$$J_{in} = \sqrt{\frac{8k_BT_i}{\pi m_i}}\frac{n_i}{4},\ J_{en}=\sqrt{\frac{8k_BT_e}{\pi m_e}}\frac{n_e}{2} - \delta\gamma J_{in},\ \varphi = 0. \tag{2.4}$$

The conditions for the ions and the electrons are similar to the ones for the dielectric wall (2.2), except for the second term on the rhs of the boundary condition for the electrons (the second equation in (2.4)). This term describes secondary electron emission, which may become relevant if the local electric field is directed from the plasma to the anode. A parameter δ is introduced which is 1 if the local electric field is directed to the anode, and 0 otherwise. Note that the choice of which secondary electron emission coefficient, γ, to use was not clear as the anode sheath voltage and, consequently, the energy of incident ions are small. In any case, this term produces a small effect even for γ of order unity, since its magnitude for comparable n_i and n_e is of the order of $\gamma\sqrt{m_eT_i/\left(m_iT_e\right)}$ with respect to the first term on the rhs of the second equation in (2.4). The third condition in (2.4) defines the zero of potential.

The boundary $z = h$ is positioned in the discharge column, where the charged species densities are independent of z and the axial electric field is constant (independent of r, ϕ, z):

$$\frac{\partial n_i}{\partial n} = 0, \frac{\partial n_e}{\partial n} = 0, \quad \frac{\partial \varphi}{\partial n} = E_z. \tag{2.5}$$

Here E_z is the axial electric field; a given parameter which may be chosen to ensure desired values of the discharge current I. The parameter h has to be large enough so the conditions (2.5) are satisfied not just at the boundary $z = h$, but also in a region adjacent to the boundary; in other words, h has to be larger than the thickness of the near-anode region.

We hypothesize that the problem (2.1)-(2.5) admits an axially symmetric (2D) steady-state solution, describing a spotless, or diffuse, mode of current transfer to the anode, and three-dimensional steady-state solutions, presumably describing modes with patterns of spots. By analogy with computed spot patterns on cathodes of DC glow discharges, and in qualitative agreement with experimental results on anode spot patterns, we assume that the 3D solutions are periodic in ϕ with the period $2\pi/n$, where $n = 1, 2, 3, \ldots$, then it is sufficient to limit the computation domain to a half-period of the desired 3D solution: $0 \leq \phi \leq \pi/n$. Boundary conditions at $\phi = 0$ and $\phi = \pi/n$ are zero normal derivatives,

$$\frac{\partial n_i}{\partial n} = 0, \frac{\partial n_e}{\partial n} = 0, \quad \frac{\partial \varphi}{\partial n} = 0, \tag{2.6}$$

so that $\phi = 0$ and $\phi = \pi/n$ represent planes of symmetry of the solution considered.

Results reported in this work refer to a discharge in helium under the pressure of 5 Torr. The (only) ionic species considered is He_2^+. The transport and kinetic coefficients are the same as in [84]. The discharge tube radius is $R = 0.5$ mm and the height of the computation domain is $h = 5$ mm. It is set that $\gamma = 0.03$, $T_e = 1$ eV, and $T_i = 300$ K.

The modelling was performed in COMSOL Multiphysics. Both the steady-state and time-dependent forms of problem (2.1)-(2.6) have been solved. The Plasma Module with a stationary solver, and a time-dependent solver, have been employed. The Plasma Module was adapted so that it could be used in combination with a stationary solver and supplemented with a residual-based stabilization method.

2.3 Results and discussion

One of the computed solutions reported in this chapter is 2D and describes the spotless mode. As an example, a 3D mode with $n = 8$ is also reported, and it describes a mode with eight spots. Note that the relatively high value of n permits a relatively small computation domain and thus reduces the required RAM and computation time.

The 2D solution was computed in a standard way by means of a stationary solver. It has been found in this work that 3D solutions do not bifurcate from the 2D solution,

in contrast to solutions describing cathodic spots and patterns of cathodic spots in arc and glow discharges, which do bifurcate from a fundamental (generally 2D) solution. Therefore the approach developed for the systematic computation of multiple solutions describing spots and patterns on cathodes of arc and DC glow discharges [83] could not be used. To find the 3D solution reported in this work, we first solved the 1D axially symmetric and steady-state form of the problem (2.1)-(2.2), describing the discharge column. (Analytical solutions of this 1D problem for the limiting cases corresponding to free-fall and ambipolar diffusion [22] and a recombination-dominated discharge were used to validate the code.) In order to obtain the 3D solution, a solution of the 1D problem governing the column for the discharge current $I = 10\,\mathrm{mA}$ was introduced as an initial condition for the time-dependent solver, the one solving the time-dependent form of the problem (2.1)-(2.6) including surface charge accumulation at the dielectric wall, equation (2.3). The computations have been performed with the value of E_z, the input parameter describing the axial electric field at the column boundary, corresponding to the $I = 30\,\mathrm{mA}$, and not to $10\,\mathrm{mA}$. The time-dependent solver was ran; the mismatch in E_z introduced a perturbation to the system that resulted in an evolution to a 3D time-independent solution to the problem. The stationary solver was then used to compute the 3D solution in a wide range of current.

2.3.1 Current-voltage characteristics of the anode region

Consider the potential distribution in the discharge column, φ_c, (which is axially symmetric),

$$\varphi_c\,(r,z) = -(z-h)E_z + \varphi_h\,(r)\,, \tag{2.7}$$

where $\varphi_h\,(r)$ is the distribution of potential at the computational boundary, $z = h$. We define the near-anode voltage drop as the difference between the potential at the anode (equal to zero), and the potential that is obtained by extrapolation of the column solution (2.7) to the anode ($z = 0$):

$$U = -hE_z - \varphi_h\,(r)\,. \tag{2.8}$$

Note the second term on the rhs of this definition depends on r. In order to remove the dependence on r and find an integral characteristic, one has, for example, to evaluate the rhs of equation (2.8) on the axis, or edge, of the discharge tube, or take an average value over the cross section. However, whatever choice is made is irrelevant in so far as a graphical representation of multiple solutions is concerned: different solutions with the same discharge current will coincide in the column to the accuracy of a shift of potential by a constant. Therefore, whatever way is chosen to evaluate the rhs of equation (2.8), as long as it is the same for different solutions, the difference

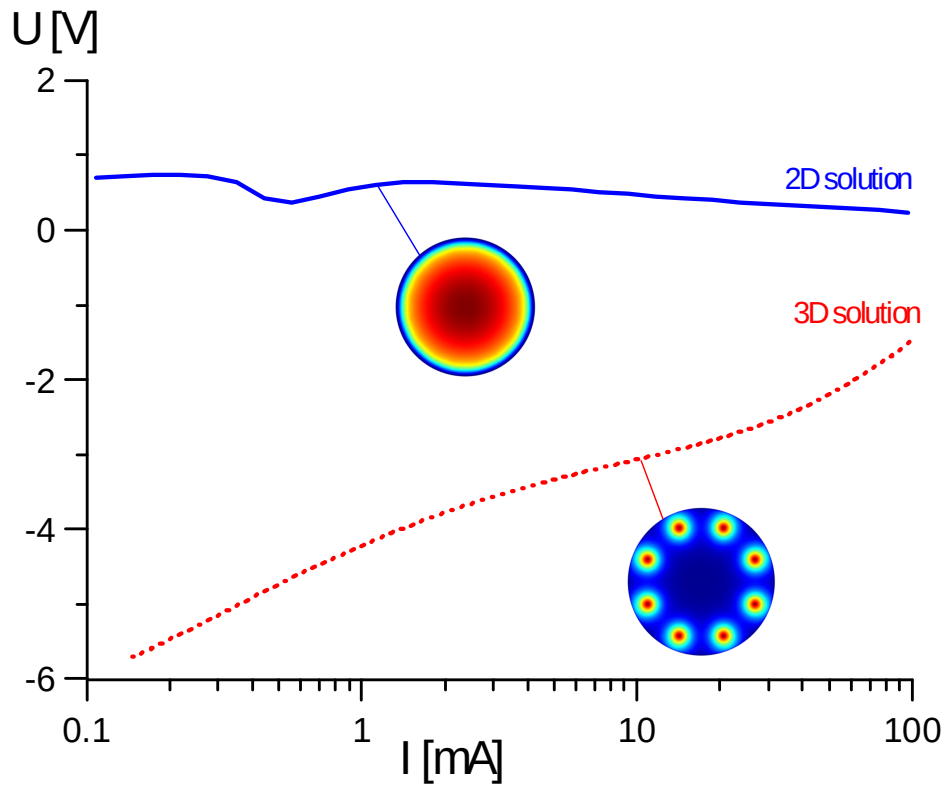

Figure 2.1: Near-anode voltage drop for a wide range of currents. Solid line: 2D mode. Dotted line: 3D mode. 2D and 3D solutions are with schematics that indicate a characteristic distribution of electron number density on the anode.

in U between the different solutions will be equal. We indicate for definiteness that in this work the rhs of equation (2.8) is evaluated on the axis.

The near-anode current-voltage characteristics (CVCs) of the two solutions, existing in the same range of current, are shown in Figure 2.1. One solution describes a 3D mode that is azimuthally periodic, the other a 2D mode that is axially symmetric. The 3D mode has a negative value of near-anode voltage in the range of the computed current, while the 2D mode has a positive value of near-anode voltage in the range of the computed current.

It is of interest to compare the CVCs in Figure 2.1 to the computed CVCs for DC glow discharges with self-organized cathode spots (e.g. Figure 3 of [85]). In the case of the cathode spots there is an N-shaped CVC corresponding to the 2D solution, with the CVC corresponding to the 3D solutions branching off from near the falling section of the CVC of the 2D solution; as per the general pattern of self-organization in bistable nonlinear dissipative systems with a positive feedback. The CVCs shown in Figure 2.1 are very different: no pronounced N-shape CVC was computed for the

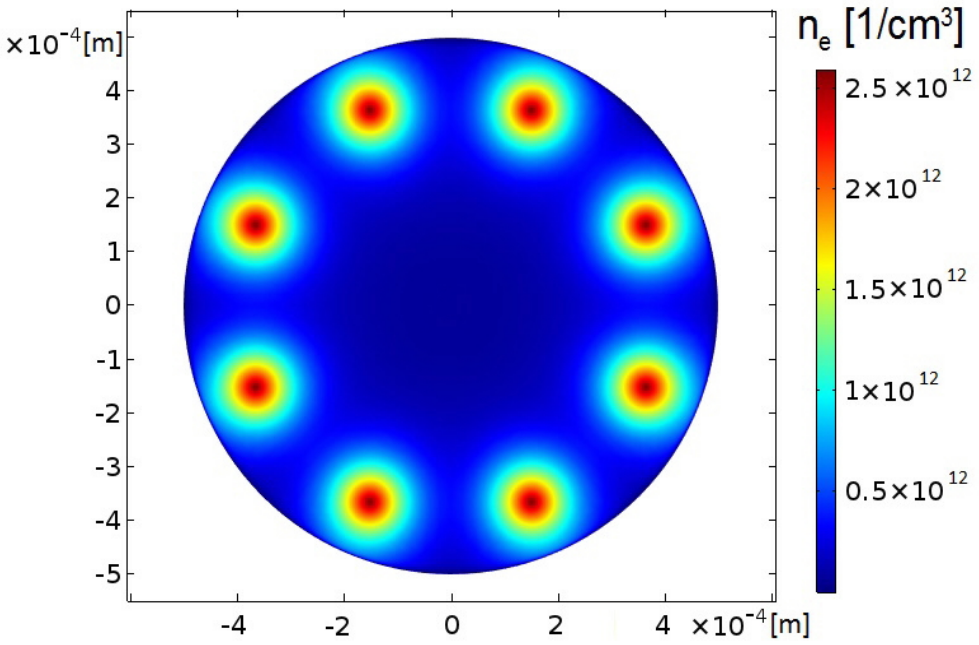

Figure 2.2: Electron number density on the surface of the anode. 3D solution, I=10 mA.

2D solution, and no bifurcations were found in a wide current range.

2.3.2 Anode spot structure

The electron number density on the surface of the anode for the 3D mode at 10 mA is shown in Figure 2.2. Electron density is organized in an azimuthally periodic pattern of spots. The pattern is similar to that observed experimentally in Figure 1 of [65].

Densities of ions and electrons are shown in Figure 2.3 in the plane of symmetry plane $\phi = 0$ (a longitudinal cross section passing through the tube axis and the centre of a spot) for $I = 1$ mA. One can see that the electron and ion densities are distributed in a similar way to the so-called fireballs observed experimentally in [76].

Distribution of the charged particle densities along the axial direction from the centre of a spot to the end of the calculation domain (a 1D plot with constant ϕ, r), for the 3D mode at $I = 0.1$ mA and 35 mA, are shown in Figure 2.4. There is a region with $n_i > n_e$, i.e., an ion sheath, adjacent to the electrode. The ion densities in the sheath are of the same order of magnitude for the two discharge currents, while the densities of the charged particles in the column vary by more than an order of magnitude. For $I = 0.1$ mA, charge separation is seen also in the column, which is due

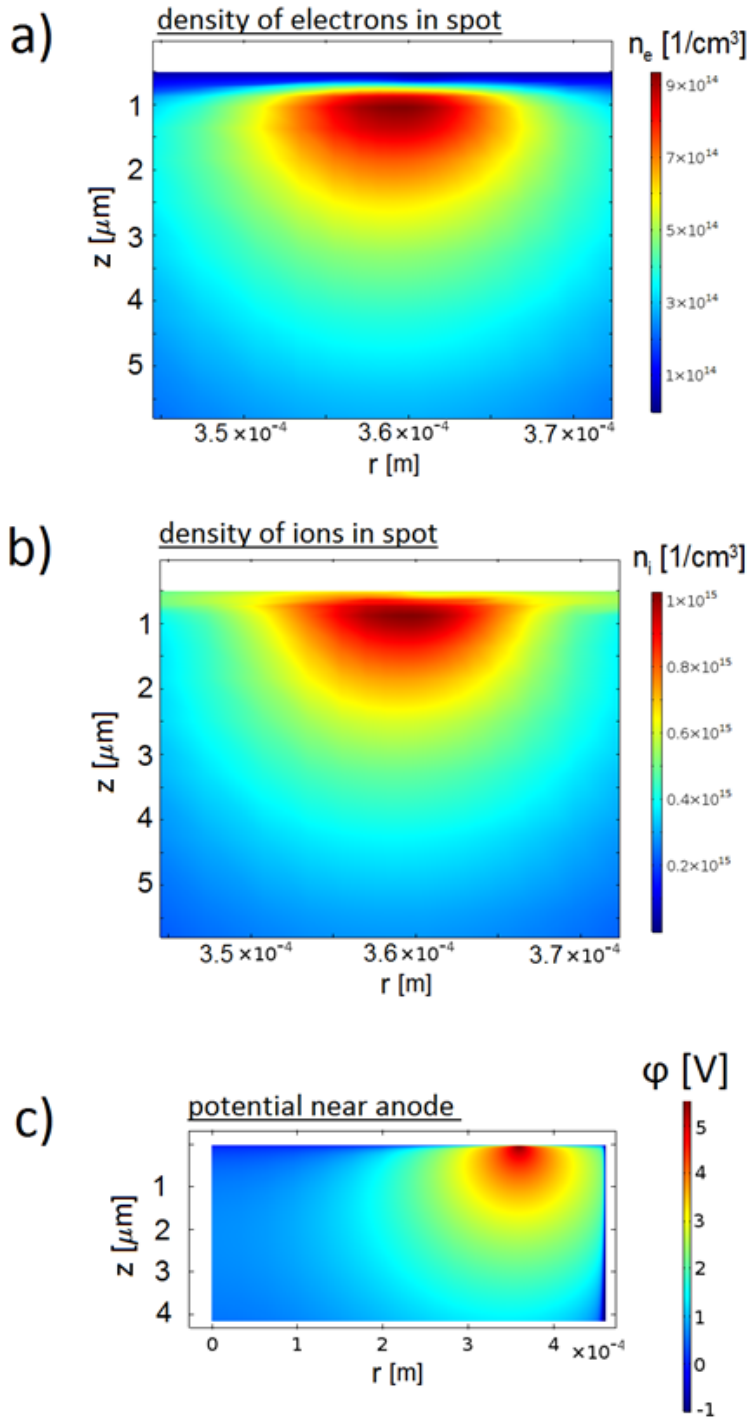

Figure 2.3: a) Electron number density in the spot. b) Ion number density in the spot. c) Electric potential in the near-anode region. Distributions in the plane of symmetry passing through the spot center. I = 1 mA.

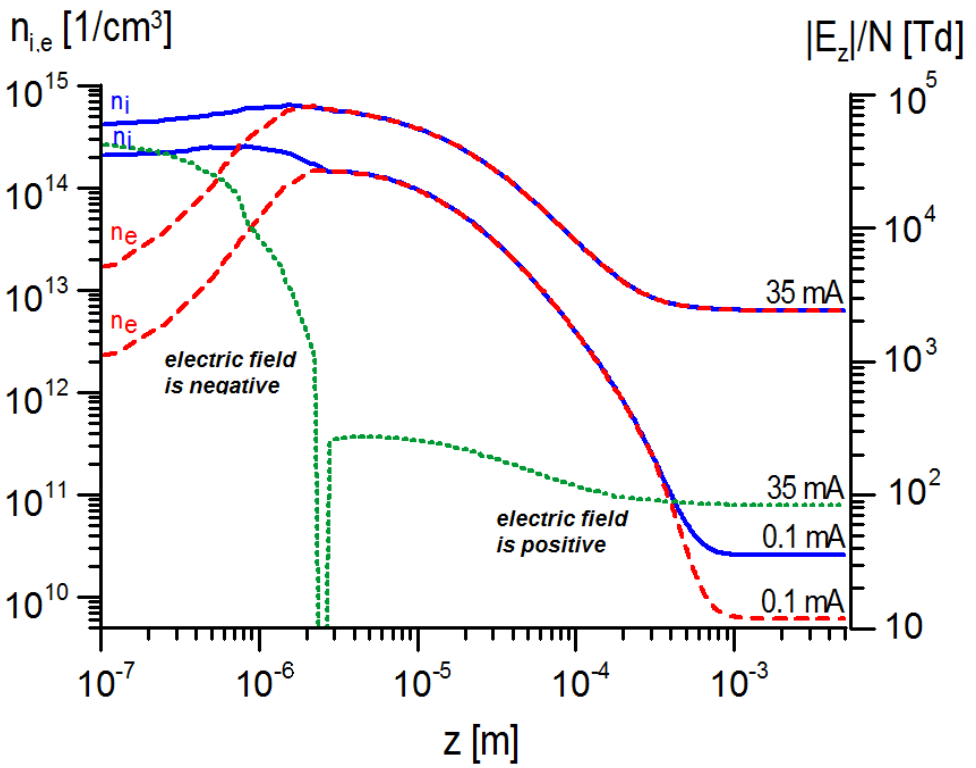

Figure 2.4: Number density of ions (solid line), number density of electrons (dashed line), for I= 35 mA, and I=1A. Reduced electric field (dotted line) for I= 35 mA. Plot made from centre of spot, along axial direction, to end of calculation domain.

to ambipolar diffusion coming into play near the (absorbing) lateral wall.

Distribution of the electric field in Figure 2.4 is shown for 35 mA. The electric field in the ion sheath is two orders of magnitude greater than that in the quasi-neutral region. The former points towards the anode, while the latter points away from the anode.

An investigation into the type of sheath that forms on a small electrode in contact with plasma, based on 2D particle-in-cell simulations, was carried out in [86]. It was shown that an electrode biased between 0 and $kT_e/2e$ below the plasma potential had quasi-neutral plasma extended to the electrode. For an electrode biased above the plasma potential, an electron sheath would be present. It is seen in Figure 2.3 c) that near the spot, the electrode is biased below the potential of adjacent plasma, and it is seen from Figure 2.4 that quasi-neutral plasma is extended close, up to 1 μm, to the electrode. In the spotless mode at the same current, the electrode potential is above that of the adjacent plasma and the electron sheath extends 50 μm from the electrode. It is seen from Figure 2.3 c) that the electrode has a positive bias with respect to

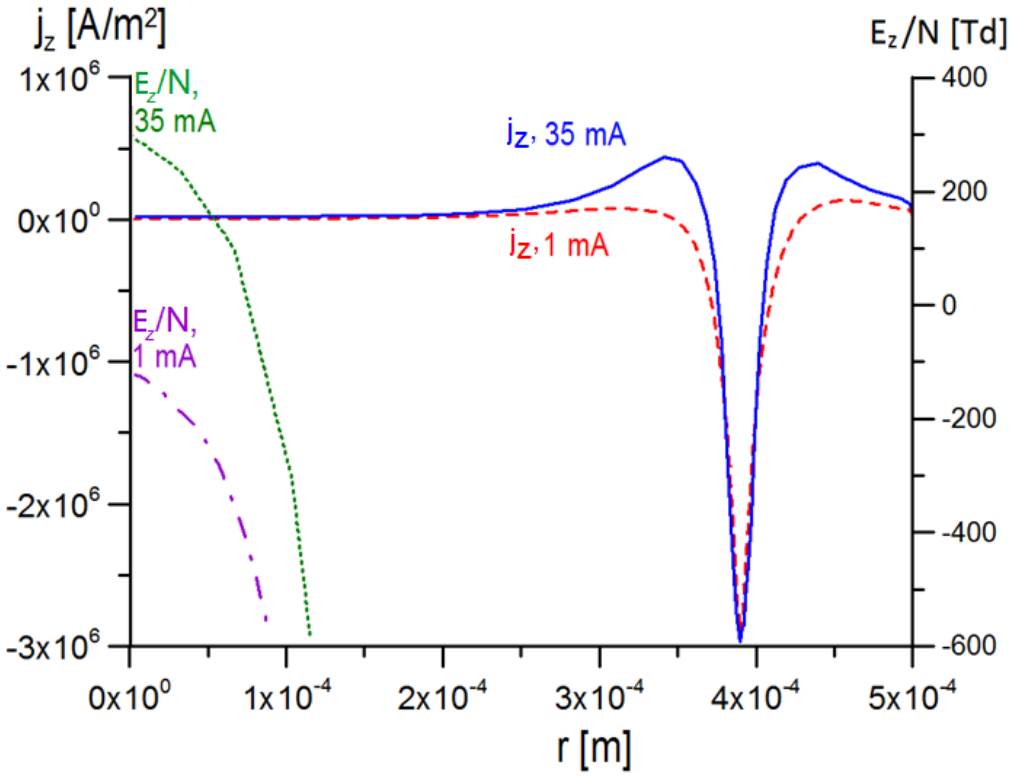

Figure 2.5: Distribution of axial current density and axial electric field on the surface of the anode in the plane of symmetry passing through the spot center. Large negative values of electric field are not shown.

the adjacent plasma large distances from the spot; skipping for brevity results on the charge particle distribution, we only note that there is an electron sheath adjacent to the electrode.

2.3.3 Near-anode physics

The distribution of current density and electric field along the anode surface in the plane of symmetry $\phi = 0$ (the longitudinal cross section that passes through the centre of a spot) is shown in Figure 2.5. Plots are included for two different discharge currents. The current density has a large magnitude and is negative inside the spot, and turns positive outside. The spot behaves like a mini-cathode or, as one could say, operates as a unipolar glow discharge.

The direction of current density in the plane of symmetry is shown in Figure 2.6. For reference the distribution of the ions number density is shown as well. The unipolar glow discharge is clearly seen.

The electric field at the anode in Figure 2.5 is seen to be both negative inside the

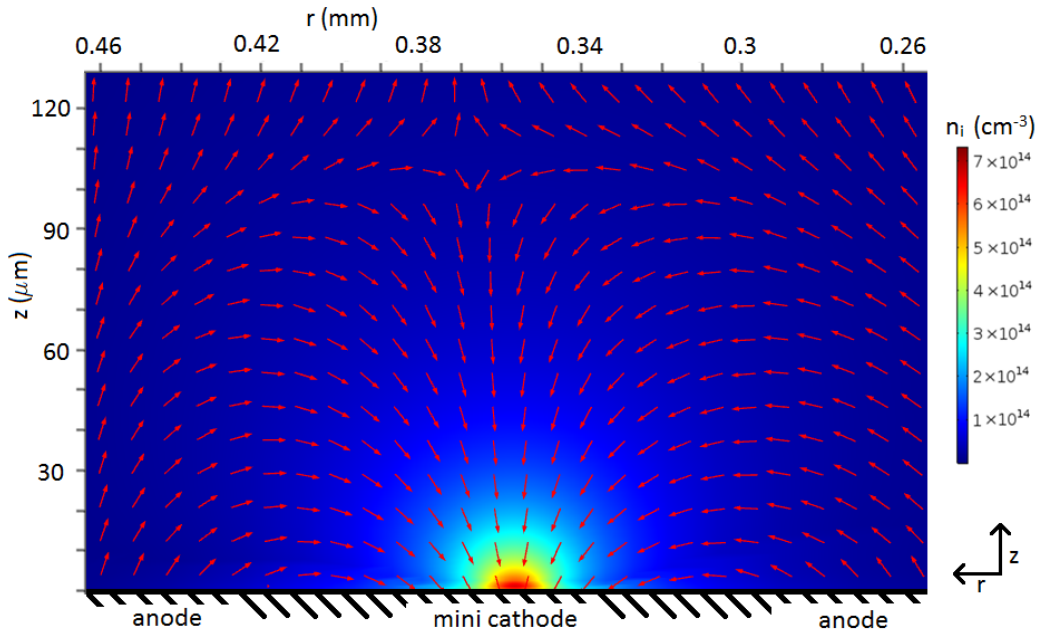

Figure 2.6: Distribution of the number density of ions in the plane of symmetry passing through the spot center. Arrows: unit vector of current density. I=1 mA.

spot and positive outside for 35 mA; it is negative everywhere for 1 mA. Directions of the electric field at the anode and of current density from the anode inside and outside the spot are summarized in Table 2.1. For the 2D spotless mode, $E_z > 0$, $j_z > 0$ for all values of current.

Current	3D, within the spot	3D, outside the spot
1 mA	$E_z < 0$, $j_z < 0$ (cathode)	$E_z < 0$, $j_z > 0$ (field-reversal anode)
35 mA	$E_z < 0$, $j_z < 0$ (cathode)	$E_z > 0$, $j_z > 0$ (regular anode)

Table 2.1. Physics of the near-anode region for the 3D solution.

2.3.4 Additional comments

No double layers were found during this modelling. However, this modelling was performed at a higher pressure than the pressure of the experiments that revealed double layers. An interesting question is whether the self-organised anode spots reported here would contain double layers at lower pressure, or if they are distinct phenomena.

The modelling reported in this work should not be interpreted as an attempt to quantitatively describe parameters of anode spots. Merely, the aim was to prove the possibility of self-consistently describing self-organized anode spots on the basis of

multiple solutions existing in the same range of discharge currents, which was achieved. The model may be used for qualitative analysis, and certainly some interesting trends have emerged. Nevertheless it is well known that a detailed account of the complex plasma chemistry of a helium discharge, and the nonlocality of electron energy ought to be included. Another aspect that needs to be improved is a description of the near-electrode sheath, which is collisionless inside the spot.

Bombardment on the anode by low-kinetic energy ions occurs inside the spots. An interesting hypothesis is that the ions incident on the anode contribute to or are responsible for the cancer-inhibiting effect reported in [81].

2.4 Conclusions

For the first time, a self-organized pattern of spots of plasma on an anode was computed self-consistently. A new class of stationary solutions, describing anode spots, was found in the conventional DC glow discharge model. The 3D solution was found to exist in the same range of currents as a 2D solution describing a spotless mode of current transfer.

On the one hand, there are similarities between the computed anode spots and the spots on cathodes of arc and DC glow discharge: both are described by multiple steady state solutions and reveal azimuthal periodicity. On the other hand, the spots on the anode are different to the spots on the cathode in following ways: the solution describing the spotless mode does not contain a pronounced N-shaped current-voltage characteristic; no bifurcations were found in a wide range of currents, i.e., the anode spots were found to exist isolated from the 2D spotless mode. The anode spots are apparently related to the change in the sign of the near anode voltage.

Inside the spots the anode behaves like a mini-cathode, in that the sign of the current density and electric field is reversed. In other words, anode spot operates as a unipolar glow discharge.

Chapter 3

Modelling cathode spots in glow discharges in the cathode boundary layer geometry

3.1 Introduction

Self-organized patterns of cathode spots in DC glow microdischarges were observed for the first time in 2004 [46] and represent an important and interesting phenomenon. A range of experimental reports have since been published [7, 46–54]. Modelling of the phenomenon [42, 43, 53, 56–58] has revealed, in agreement with the general theory of cathode spots and patterns in arc and DC glow discharges [63], the existence of multiple steady-state solutions for a given value of discharge current, which comprise modes of current transfer associated with different cathode spot patterns. Predictions concerning the existence of self-organized patterns in gases other than xenon, generated from the modelling, have been confirmed experimentally [53].

The vast majority of the experiments [7, 46–54] have been performed in a discharge device comprising a flat cathode and a ring-shaped anode, separated by a dielectric (cf., e.g., Figure 1 of [54]); this discharge configuration is called cathode boundary layer discharge (CBLD) by the authors of the experiment. However, the modelling has been performed up to date for discharges with parallel-plane electrodes only [42, 43, 53, 56–58]. The question of how the shape of the anode affects the pattern of self-organization has so far not been addressed. Furthermore, the effect over 3D spots of absorption of the charged particles by a dielectric surface has not been investigated in full due to computational difficulties [57].

In this work, 3D modelling of cathode spots is reported for the first time in CBLD, and the self-organization is computed with a full account of absorption of charged

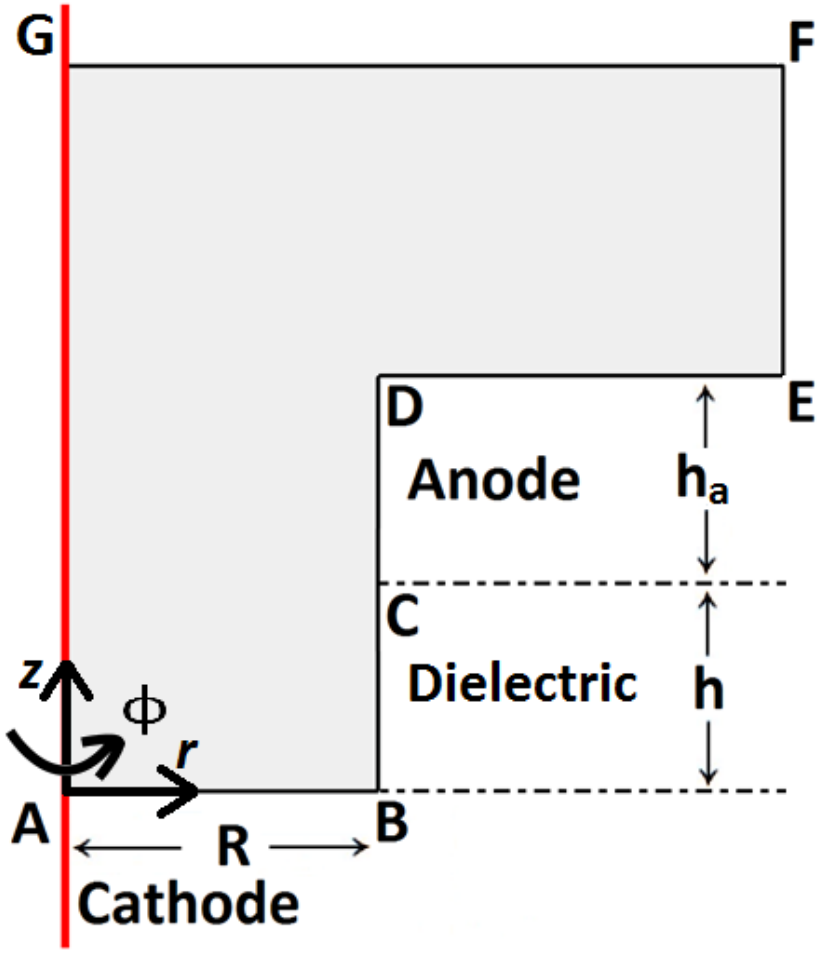

Figure 3.1: Configuration of a cathode boundary layer vessel. AG is the axis of symmetry of the vessel.

particles at the dielectric surface. The outline of the chapter is as follows. The model is described in section 3.2. In section 3.3.1 the effect over the fundamental mode of the discharge radius, the thickness of the cathode and dielectric, and of a dielectric surface that reflects charged particles is investigated. In section 3.3.2 examples of computed 3D modes are given and compared to their experimental counterparts, the effect on 3D modes of a dielectric surface that reflects charged species is also analyzed. In section 3.4 conclusions are drawn.

3.2 Model and Numerics

The model employed in this work is the most basic self-consistent model of glow discharge. Although the model is very well-known, it is described here for the sake of completeness. The model comprises equations for conservation of electrons and a single ion species, written in the drift-diffusion transport approximation, and Poisson's equation:

$$\begin{aligned} \nabla \cdot \mathbf{J}_i &= n_e \, \alpha \, \mu_e \, E - \beta \, n_e \, n_i, \quad \mathbf{J}_i = -D_i \, \nabla n_i - n_i \, \mu_i \, \nabla \varphi, \\ \nabla \cdot \mathbf{J}_e &= n_e \, \alpha \, \mu_e \, E - \beta \, n_e \, n_i, \quad \mathbf{J}_e = -D_e \, \nabla n_e + n_e \, \mu_e \, \nabla \varphi, \\ \varepsilon_0 \, \nabla^2 \varphi &= -e \, (n_i - n_e) \, . \end{aligned} \tag{3.1}$$

Here n_i, n_e, $\mathbf{J}_i$, $\mathbf{J}_e$, D_i, D_e, μ_i, and μ_e are number densities, charged species transport fluxes, diffusion coefficients, and mobilities of the ions and electrons, respectively; α is Townsend's ionization coefficient; β is coefficient of dissociative recombination; φ is electrostatic potential, $E = |\nabla \varphi|$ is electric field strength; ε_0 is permittivity of free space; and e is elementary charge. The local-field approximation is employed (i.e. electron transport and kinetic coefficients are assumed to depend on the local electric field only).

Boundary conditions at the cathode and anode are written in the conventional form. Diffusion fluxes of the attracted particles are neglected as compared to drift; the normal flux of the electrons emitted by the cathode is related to the flux of incident ions in terms of the effective secondary emission coefficient γ, which is assumed to characterize all mechanisms of electron emission (due to ion, photon, and excited atom bombardment) [2]; density of ions vanishes at the anode; electrostatic potentials of both electrodes are given. The dielectric surface is electrically insulating, and absorbs the charged particles (i.e. case *i)* $n_i = n_e = 0$); for comparison, some solutions were computed for the case of a reflecting dielectric surface (i.e. case *ii)* $\frac{\partial n_i}{\partial r} = \frac{\partial n_e}{\partial r} = 0$). With the computational domain from Figure 3.1, the boundary conditions read

$$\begin{aligned}
&\text{cathode } (AB): \quad \tfrac{\partial n_i}{\partial z} = 0, \quad J_{ez} = -\gamma J_{iz}, \quad \varphi = 0\,; \\
&\text{anode } (CDE): \quad n_i = 0,\ \tfrac{\partial n_e}{\partial n} = 0\,, \quad \varphi = U; \\
&\text{dielectric } (BC): \quad \begin{matrix} i)\ n_i = n_e = 0 \\ ii)\ \frac{\partial n_i}{\partial r} = \frac{\partial n_e}{\partial r} = 0 \end{matrix}\ , \ J_{er} - J_{ir} = 0; \\
&\text{numerical boundary (EFG)}: \quad n_i = n_e = 0\ , \quad \tfrac{\partial \varphi}{\partial n} = 0.
\end{aligned} \tag{3.2}$$

Here U is the discharge voltage, the subscripts r and z denote radial and axial projections of corresponding vectors, and $\partial/\partial n$ means a normal derivative. The lengths DE and AG are large enough so that boundaries EF and FG do not affect the solution**;** simulations were run also with a smaller calculation domain (lengths DE and AG were reduced) and no significant differences in the solutions were observed. The results reported in this work refer to $h = 0.5\,\text{mm}$, $h_a = 0.1\,\text{mm}$, and $R = 0.5\,\text{mm}$ unless indicated otherwise.

The control parameter can be either discharge voltage U or discharge current I, depending on the slope of the current voltage-characteristics (CVC) $U\,(I)$. In the first case, the value U of potential on the anode is set as the input parameter. In the second case, the problem is supplemented by a requirement that the discharge current takes a prescribed value and U is treated as an unknown that has to be found as a part of the solution; the calculation in this case is performed using a weak formulation in COMSOL Multiphysics.

Results reported in this work refer to a discharge in xenon under the pressure of 30 Torr. The (only) ionic species considered is Xe_2^+. The transport and kinetic coefficients are the same as in [57]. Note that a more detailed model (one that also took into account both atomic and molecular ions, excited atoms, excimers, stepwise ionization, ionization of excimers and non-locality of electron energy) was used for investigation of axially symmetric self-organized patterns in the parallel-plane configuration [57] and gave patterns qualitatively similar to those predicted by the relatively simple model described in this section. On the other hand, the simple model results in significantly reduced computation time, which was essential when performing 3D modelling. Therefore, the simple model was seen as adequate for the purpose of investigating the effect of CBL discharge configuration.

The problem (3.1) to (3.2) admits multiple solutions describing different discharge modes. One such mode exists for all ranges of current, it is 2D (axially symmetric) and termed fundamental, this is routine to calculate. 3D modes bifurcate from (and rejoin) the fundamental mode and are termed non-fundamental modes.

To calculate non-fundamental modes, one first locates points of bifurcation on the fundamental mode by means of linear stability analysis. The procedure is discussed in detail in [43] and in brief may be described as follows. Axially symmetric 2D sta-

tionary solutions are found for the problem (3.1)-(3.2) for a wide range of currents. Azimuthally periodic perturbations with an exponential time dependence are introduced. The time-dependent form of problem (3.1)-(3.2) is then linearized and assumes the form of an eigenvalue problem for a set of linear homogeneous differential equations, the perturbation increment λ being the eigenparameter. For each current and each azimuthal period, the problem is solved by means of the eigenvalue solver of COMSOL Multiphysics. Bifurcations are found at currents where λ vanishes.

Next a 3D calculation domain is created by rotating the 2D domain $ABCDEFG$ from Figure 3.1 about the axis AG of symmetry of the discharge vessel, by an angle equal to half of the azimuthal period of the 3D mode being sought. The beginning of the non-fundamental mode is then searched for on the fundamental mode, with the 3D calculation domain, in the vicinity of the bifurcation point predicted by the linear stability analysis. Small azimuthally periodic perturbations are introduced to the densities of charged species at the bifurcation point; the stationary solver's iterations will eventually converge to the 3D mode. The remainder of the 3D mode is straightforward to calculate.

The above procedure was realized using stationary and eigenvalue solvers from the commercial product COMSOL Multiphysics. The meshes used were considered appropriate when after increasing their refinement the solutions were not significantly affected. The time taken by the stationary solver to find convergence to one of the most computationally intensive 3D solutions is around 1 hour, with a computer with a Intel Core i7-4770 CPU at 3.4 GHz and 32 GB of RAM.

3.3 Results

3.3.1 Fundamental mode

In Figure 3.2, the CVC of the fundamental mode is displayed in four sets of conditions, labeled 1 to 4 in the Figure. Surprisingly, two turning points and a loop are present on the CVC corresponding to the baseline conditions ($h = 0.5\,\text{mm}$, $h_a = 0.1\,\text{mm}$, and $R = 0.5\,\text{mm}$, absorbing dielectric surface), line 1.

The whole current range in Figure 3.2 can be divided into three regions, marked I, II, III. At the top of the Figure there is an illustration of the characteristic distribution of current density on the cathode surface for each region. The color range shown in the bar is used also for the rest of the document. The general pattern of evolution of the fundamental mode with increasing current is as follows. In region I, corresponding to the Townsend discharge, the current is distributed on the cathode in the form of a ring. In region II, the ring of current grows thicker with increasing current. In region

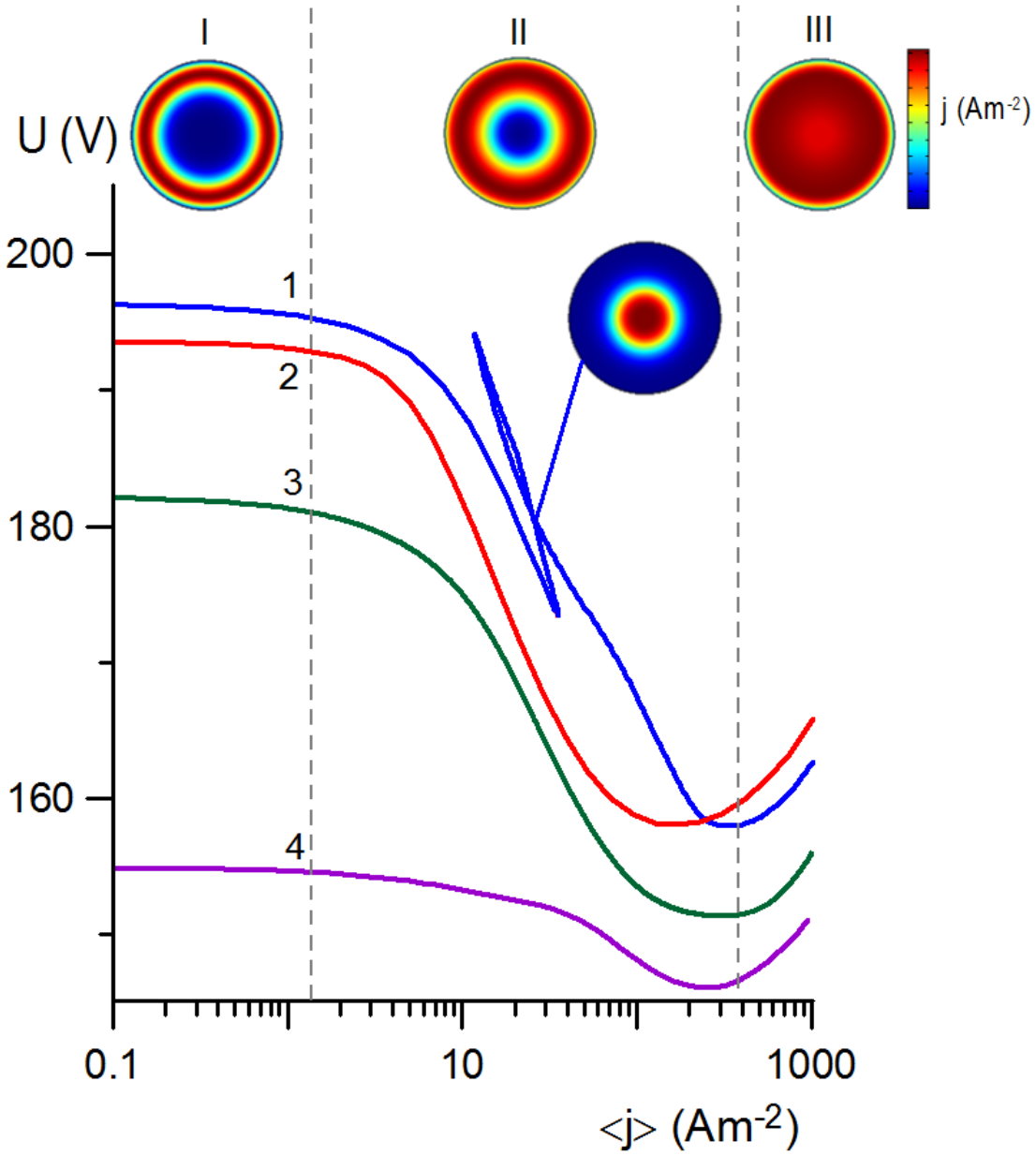

Figure 3.2: Fundamental mode. 1: baseline conditions. 2: h = 0.5mm, h_a = 0.1mm, R = 1.5mm. 3: baseline geomentry, reflecting dielectric surface. 4: h =0.25mm, h_a = 0.25mm, R = 0.375mm.

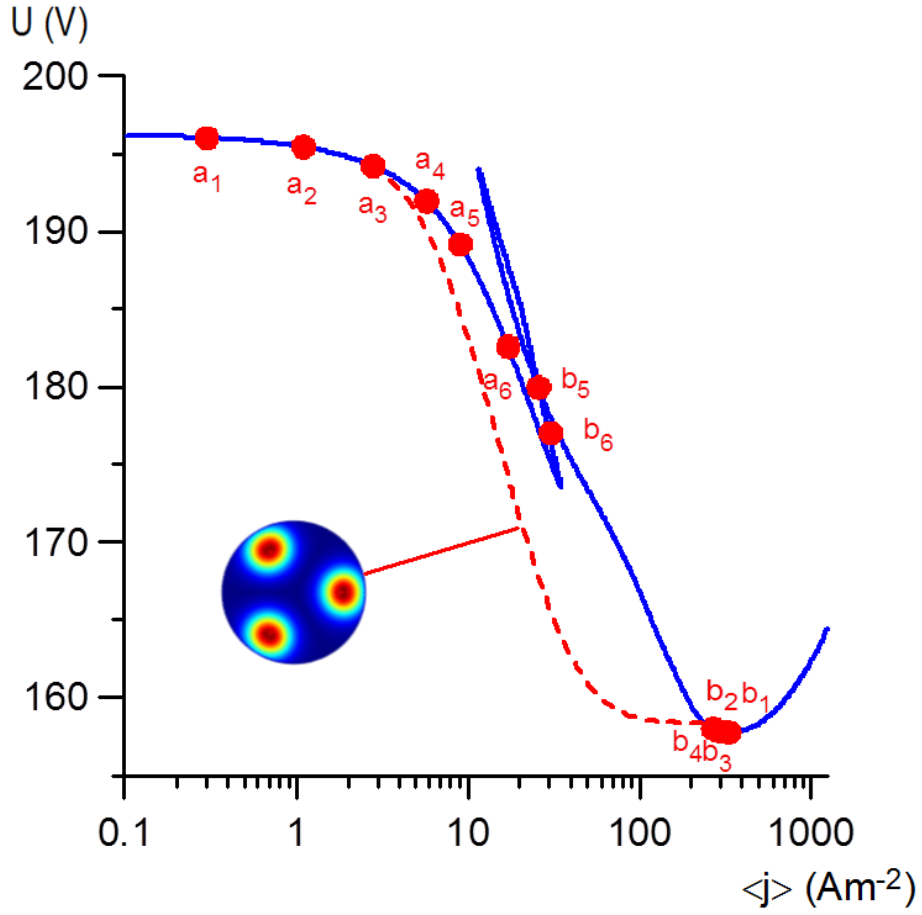

Figure 3.3: Solid: fundamental mode (mode 1 of figure 2). Dashed: mode a_3b_3. Circles: points of bifurcation.

III, corresponding to the abnormal discharge, the discharge fills most of the cathode surface.

In the case represented by line 1, a pattern with a central spot appears on the section between the turning points, as indicated in the Figure. This transition is accompanied by a loop in the CVC. The loop is absent in the CVC of cases 2 and 3; the larger radius and the reflecting dielectric surface, respectively, prevent the transition from a ring to central spot. The loop is also absent in the CVC of case 4. The CVC of cases 1, 2 and 4 (the ones with absorbing dielectric surface) have small humps in range I, although this cannot be seen in the scale of Figure 3.2.

3.3.2 3D modes

Figure 3.3 displays the CVC of the fundamental mode for the baseline conditions, points of bifurcation of 3D modes, and an example 3D mode. Each pair of points a_i and b_i designates from where a 3D mode branches off from and rejoins the fundamental mode. Mode $a_i b_i$ possesses period $2\pi/i$, meaning that $a_1 b_1$ possesses azimuthal period 2π, mode $a_2 b_2$ possesses azimuthal period π, and so on. Bifurcation points b_1 to b_4 virtually coincide. Points b_5 and b_6 are positioned on the section between the turning points. The 3D modes branch off and rejoin the fundamental mode in a palindromic order along current, which conforms to previous modelling of discharges with parallel-plane electrodes.

As an example, the CVC of mode $a_3 b_3$ is shown in Figure 3.3. (The schematic in the figure illustrates the pattern of spots associated with this mode.) The CVC manifests a plateau between $60\,\mathrm{A\,m^{-2}}$ and $300\,\mathrm{A\,m^{-2}}$, which is a manifestation of the normal current density effect. Note that the plateau also is present in the computed mode of the same azimuthal period for a vessel with parallel-plane electrodes and reflecting dielectric surface [58].

CVCs of several different modes would be difficult to distinguish in Figure 3.3. A more convenient representation is shown in Figure 3.4: the fundamental and four non-fundamental modes are mapped in the plane $(\langle j \rangle, j_c)$, where j_c is the value of current density at the position $r = 0.4$ mm on the upper vertical radius as marked by a cross on one of the images in Figure 3.4. Note that the value $r = 0.4$ mm coincides with the radius of the ring associated with the fundamental mode in the Townsend regime; it was found that such a choice ensures maximum distinction between the modes. Following the fundamental mode from low to high currents, it is seen that j_c decreases while the central spot is forming, then it increases as the ring mode forms, thus yielding a limp Z-shape on the bifurcation diagram. Modes $a_5 b_5$, $a_6 b_6$ possess turning points.

In Figure 3.5 the evolution is shown of patterns of current density on the cathode associated with modes $a_3 b_3$, $a_4 b_4$, $a_5 b_5$, $a_6 b_6$ from Figure 3.4 as discharge current is changed. Let us consider first the evolution of the patterns for mode $a_3 b_3$ which is shown in Figure 3.5a). The state a)i) is positioned in the vicinity of the bifurcation point b_3, the pattern is of three diffuse elongated spots, slightly deforming into a 3D structure with the period of $2\pi/3$. At a)ii) the three spots have become more distinct, intense and bean-shaped. The spots then become circular, and move farther from the center of the cathode as seen in state a)iv). The spots then once more become bean-shaped, then once again gain a triangular type structure as in state a)v). At state a)v) a central triangle-shaped 'cold spot' is present. Continuing along the mode

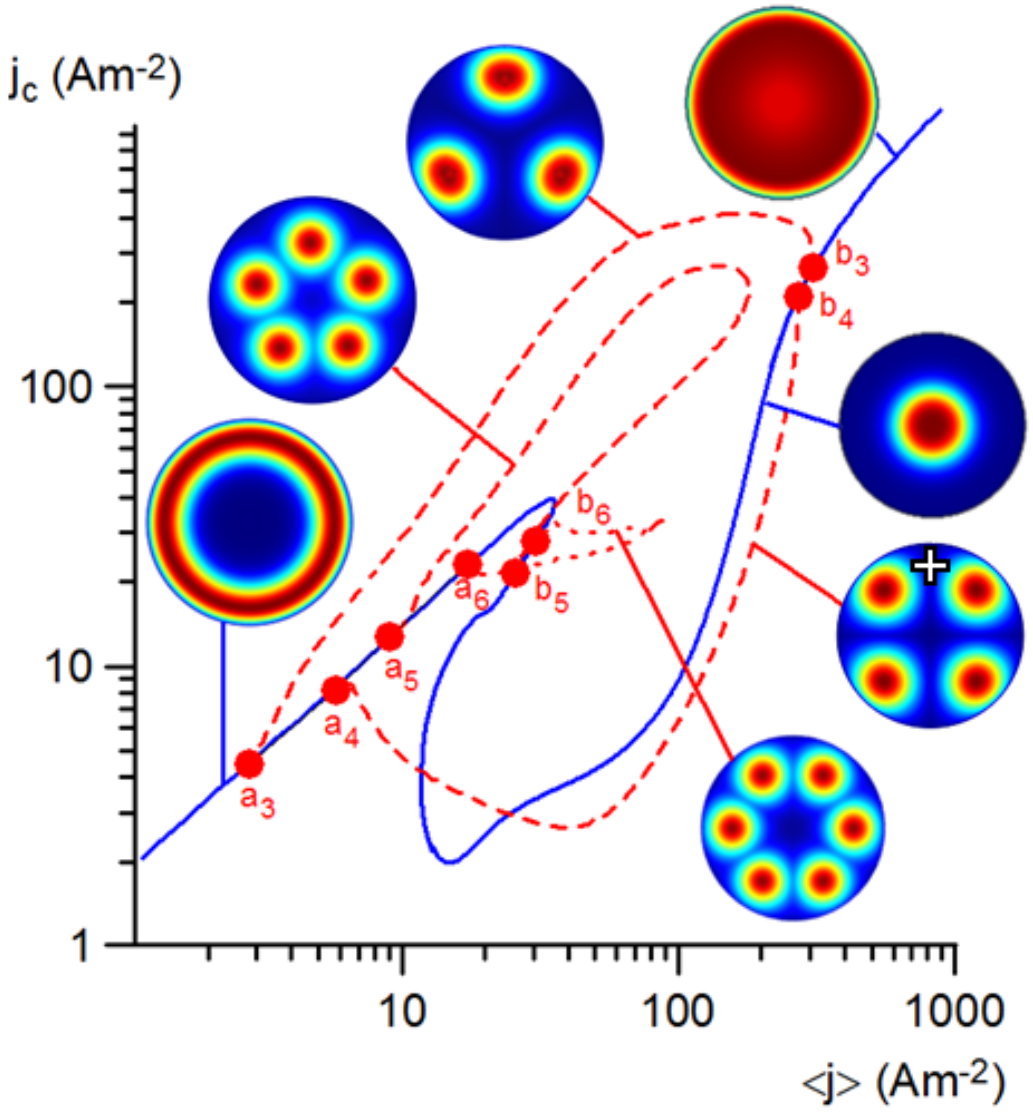

Figure 3.4: Bifurcation diagram. Solid: fundamental mode (mode 1 of figure 2). Dashed: modes a_3b_3, a_4b_4, a_5b_5. Dotted: mode a_6b_6. Circles: points of bifurcation. '+' on the image representing the mode a_4b_4 indicates the point on cathode surface where the value j_c is taken.

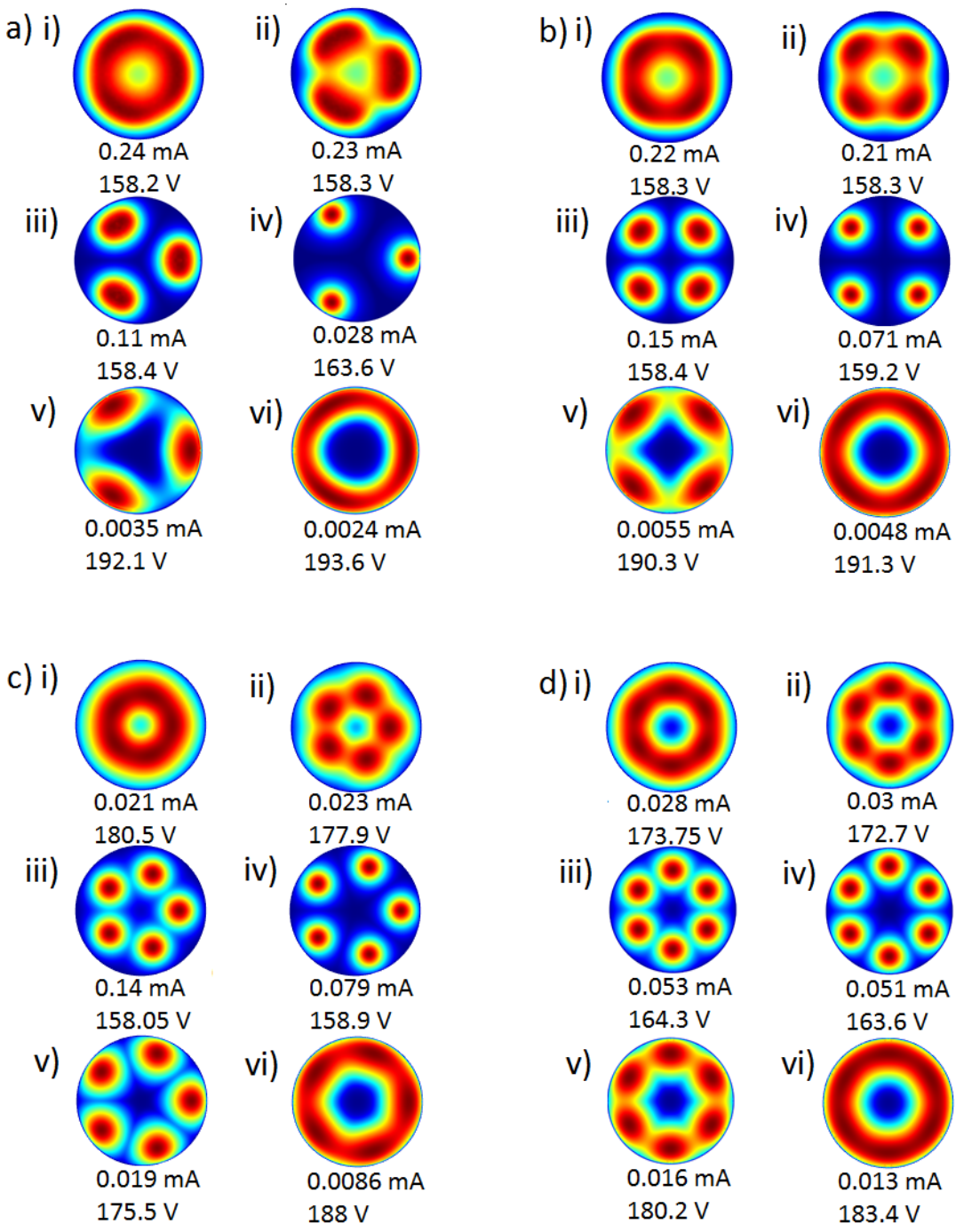

Figure 3.5: Evolution of patterns of current density on the cathode associated with 3D modes of figure 4: (a) mode a_3b_3, (b) mode a_4b_4, (c) mode a_5b_5 and (d) mode a_6b_6.

with decreasing current, the triangle shaped region becomes less sharp, and the whole pattern becomes more like the ring-shaped distribution present at a_3.

The evolution of the patterns associated with modes a_4b_4, a_5b_5, and a_6b_6, is shown in Figures 3.5b-d, respectively, follows the same trend as mode a_3b_3: first the ring is transformed into elongated bean-shaped spots and then circular spots, then they migrate to a different radius, and there, from circular spots they turn into bean-shaped spots and then merge into a different ring. No 3D modes with central hot spots were found in the present work, while in previous modelling they were; e.g. [58]. The images in Figure 3.5 can be compared to experimentally observed patterns of spots, Figure 3.2 of [54]. The computed evolution from the abnormal mode into mode a_4b_4, comprising four spots (Figure 3.5b), is in good agreement with the experimentally observed transition between the abnormal mode into a mode comprising four spots.

In Figure 2 of [54], it can be seen how the modes appear in the experiment: starting from the abnormal mode and reducing discharge current, a mode comprising four spots appears. As current is further reduced, modes comprising five and six spots appear. Further reducing current from the mode with six spots, the discharge goes back to modes with five, four, three and a ring spot. In the modelling, cf. Figure 3.3, starting from a state in the abnormal mode and following the fundamental mode in the direction of low currents, the bifurcation point b_1 of mode a_1b_1, comprising one spot, appears first. The next bifurcation point to appear is b_2 of mode a_2b_2, comprising two spots; and so on until bifurcation point b_6 of mode a_6b_6, comprising six spots, following the same trend observed in the experiment. On further following the fundamental mode in the direction of low currents, eventually the bifurcation point a_5 of mode a_5b_5 appears; and so on until a_1 of mode a_1b_1, again following the same trend as in the experiment.

In Figure 3.6, typical distributions of discharge parameters along a cross section of a hot spot are shown. Figures 3.6 a)-c) refer to state i) in Figure 3.5b) and Figures 3.6 d)-f) refer to state iv). The effect of normal current density is seen in Figure 3.6a) and 3.6c).

The patterns of current density on the cathode shown in Figure 3.3-3.5 are essentially the same as in simulations for plane-parallel electrode configurations; e.g. Figure 5 of [58]. The difference is that the spots in Figure 5 of [58] are centred at the periphery of the cathode, while the 3D spots of the present work are centred and formed totally within the cathode. The latter is what is observed in the experiments [7, 46–54]. The reason of this difference is in different boundary conditions at the dielectric surface: while modelling [58] has been performed for the reflecting surface (boundary condition ii) in the third line of equation (3.2)), the 3D spots reported in the present work have been computed for the absorbing surface (boundary condition i)). Unsurprisingly, the

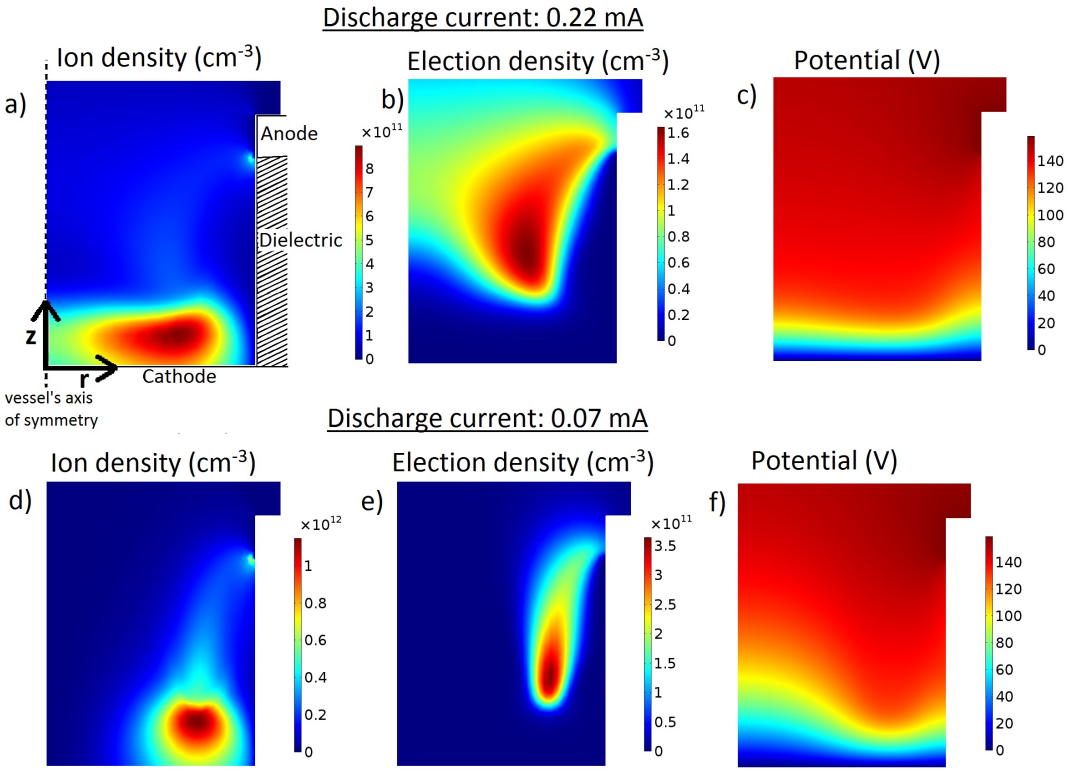

Figure 3.6: Cross section view of a 3D hot spot associated with the mode a_4b_4 at different currents. The cross section plane passes through the centre of the spot. (a), (d): Ion density. (b), (e): Election density. (c), (f): Potential.

assumption of absorbing dielectric surface, being more realistic by itself, gives results with better agreement with the experiment.

3.4 Conclusions

Self-organized 3D spot modes are reported for a typical configuration of cathode boundary layer discharge ($h = 0.5\,\mathrm{mm}$, $h_a = 0.1\,\mathrm{mm}$, and $R = 0.5\,\mathrm{mm}$) in xenon at the pressure of 30 Torr. The general form of the computed self-organized patterns is similar to those computed previously in the parallel-plane configuration and to those observed in the experiment in the sense that all of them comprise axially symmetric ring spots or circular arrangements of 3D spots. This is consistent with experimental evidence [49] that similar self-organized patterns appear in both electrode configurations.

Simulations of 3D spot patterns with the dielectric surface fully absorbing the charged particles reveal spots not centered at the periphery of the cathode, but rather located inside the cathode, as they are in the experiment. It has been found that there is a palindromic series of the number of spots with discharge current, which is consistent with observations of switching between modes with different patterns in the experiment [54].

Chapter 4

Bifurcations in the theory of current transfer to cathodes of DC discharges and observations of transitions between different modes

4.1 Introduction

Luminous spots on electrodes of direct current glow and arc discharges and self-organized patterns of spots represent a very interesting phenomenon, which is also important for applications. The presence, or not, of spots on electrodes is a key point for the operation of any arc device. Self-organized patterns appearing on cathodes of dc glow microdischarges are sources of excimer radiation [48, 51]. Self-organized patterns on liquid anodes of atmospheric pressure glow microdischarges have been shown to produce a nontrivial cancer-inhibiting effect [87].

The theoretical description of spots and spot patterns on electrodes of dc glow and arc discharges is based on the multiplicity of solutions: an adequate theoretical model must in some cases allow multiple steady-state solutions to exist for the same conditions (in particular, for the same discharge current I), with different solutions describing the spotless (diffuse) mode of current transfer and modes with different spot configurations.

Some of the multiple solutions may merge, or become identical at certain values of the control parameter; a bifurcation, or branching, of solutions. Bifurcations of differ-

ent kinds of steady-state solutions have been encountered in the theory and modelling of current transfer to cathodes of dc glow and high-pressure arc discharges [43, 63]. An understanding of these bifurcations is crucial for the computation of the whole pattern of multiple solutions and an analysis of their stability. The existence of multiple solutions and their bifurcations, in the case of current transfer to cathodes of DC glow discharges, is a consequence of a strong positive feedback, which originates in the increasing dependence of the rate of ionization on electric field. In the case of current transfer to cathodes of arc discharges, the existence of bifurcations is a result of a strong positive feedback originating in the dependence of the density of the energy flux from the plasma to the cathode surface on the surface temperature [63].

In contrast, multiple steady-state solutions describing different modes of current transfer to anodes of glow microdischarges computed recently [88] do not reveal bifurcations. The existence of multiple solutions in this case is related to the change of sign of the anode sheath voltage.

Thus, the existence, or not, of bifurcations of steady-state solutions, describing different modes of current transfer to electrodes of dc glow and arc discharges, is related to the underlying physics and is therefore of significant interest. Unfortunately, the question of whether bifurcations exist has not been addressed in experimental publications. (Although there are interesting results concerning bifurcations in the pattern of oscillations developing in a dc-driven semiconductor-gas discharge system [89]; see also [90, 91] and review [92].) It is therefore of interest to analyze available experimental observations of different modes of current transfer to electrodes of dc glow and arc discharges with the aim to eventually identify bifurcations.

The outline of the chapter is as follows. In Sec. 4.2, the general scenarios of changes between modes on electrodes of dc gas discharges and their relation to bifurcations of steady-state solutions are analyzed. Transitions of modes on cathodes of arc, and dc glow, discharges are considered in Secs. 4.3 and 4.4, respectively. The conclusions are summarized and directions of future work are discussed in Sec. 4.5.

4.2 Scenarios of transitions between different modes of current transfer to electrodes of dc discharges and their relation to bifurcations

Bifurcations of steady-state solutions manifest in experiments as transitions between modes with different spot patterns, which occur as the discharge current I is varied.

One can distinguish two scenarios for transitions between modes with different spot patterns. First, there are quasi-stationary, i.e., continuous, and, consequently,

reversible transitions between states where distributions of luminosity over the electrode surface possess different symmetries. Second, there are transitions that occur abruptly even for very small variations of I. Let us consider first the quasi-stationary transitions. All parameters of the discharge, including the discharge voltage U, vary with I continuously. In particular, the measured current-voltage characteristic (CVC) $U(I)$ is continuous. However, $U(I)$ is not smooth at $I = I_0$, where I_0 is the value of I where the distribution of luminosity over the electrode surface changes its symmetry. This transition is caused by a symmetry-breaking bifurcation that occurs at $I = I_0$, with stable states existing on both sides of the bifurcation point.

The above scenario may be illustrated by the following example. If the discharge vessel is axially symmetric, then the mathematical problem describing steady-state current transfer to the electrode admits an axially symmetric (2D) solution, describing the spotless mode of current transfer, and a 3D solution, describing a mode with a spot. (More precisely, there is a family of 3D solutions which differ one from the other by the azimuthal position of the spot. Other families of 3D solutions, describing modes with several spots, may exist as well.) It is a usual situation that the 3D spot-mode solution branches off from the 2D spotless-mode solution; a symmetry-breaking, or pitchfork, bifurcation. Note that a brief summary of information from the bifurcation theory relevant to this work can be found in Appendix of [43]; a further discussion can be found, e.g., in reviews [63, 93].

Let us designate by I_0 the value of discharge current at which the bifurcation occurs and assume for definiteness that the 2D solution is stable for $I > I_0$ and unstable for $I < I_0$. It may happen that the 3D solution branches off into the range $I < I_0$, where the 2D solution is unstable; a supercritical bifurcation. According to the general trends of the bifurcation theory, the 3D solution is stable at least in the vicinity of the state $I = I_0$ in this case. If such a situation is investigated experimentally and I in the experiment exceeds I_0, the discharge will operate in the 2D spotless mode and the luminosity distribution over the electrode surface will be axially symmetric. As I is reduced down to values below I_0, the luminosity distribution starts deviating from being axially symmetric and the deviation grows proportionally to $\sqrt{I_0 - I}$: a 3D spot starts being formed.

Let us now consider abrupt transitions. The initial and final states may be of the same or different symmetries, e.g., transitions from a 2D spotless state to states with a well developed 3D spot or a well developed 2D ring spot are both included in the consideration. Let us designate by I_0 the value of I at which the transition occurs. Since such transitions are accompanied by jumps in the discharge parameters, the measured CVC $U(I)$ is discontinuous at $I = I_0$.

There are two possible reasons for abrupt transitions. One of them is the loss

of stability of the mode that existed before a transition, occurring at $I = I_0$. If an abrupt transition occurs in a monotonic way, i.e., without temporal oscillations of the electrode luminosity and discharge parameters, in particular, discharge voltage, then the increment of the perturbations, against which the stability is lost and which normally have a symmetry lower than that of the initially existing mode, is real and vanishes at $I = I_0$. The latter means that two steady-state solutions exist in the vicinity of the state $I = I_0$: a solution describing the initially existing mode and a solution of a lower symmetry, describing the mode with the perturbations. Hence, a pitchfork bifurcation occurs at $I = I_0$. In order to illustrate this scenario, let us return to the above example and consider the case where the 3D spot-mode solution branches off into the range $I > I_0$, where the 2D spotless-mode solution is stable; a subcritical bifurcation. In this case, the 3D solution is usually unstable in the vicinity of the state $I = I_0$; e.g., Appendix of [43]. If the discharge operates in the spotless mode in the experiment and I is reduced down to values below I_0, the discharge will abruptly switch to another mode and this switching will occur in a monotonic way, i.e., without temporal oscillations.

Let us now consider the case where an abrupt transition is accompanied by temporal oscillations. The increment of the perturbations against which the stability is lost is imaginary at $I = I_0$ in this case. Hence, no steady-state solution bifurcates from the initially existing mode at the state $I = I_0$; i.e., the transition is unrelated to a bifurcation.

The other possible reason of abrupt transitions is that the mode that existed before the transition has a turning point at $I = I_0$. In other words, this mode has two distinct branches, which exist in the range $I \leq I_0$ (or $I \geq I_0$) and merge at $I = I_0$, so the mode does not exist for $I > I_0$ (or, respectively, $I < I_0$). One can say that the mode has reached the limit of its existence region at $I = I_0$ and turned back; a fold, or saddle-node, bifurcation. If the discharge operates on one of the branches of this mode and the current is increased (or, respectively, decreased), the discharge will abruptly switch to another mode as the value $I = I_0$ has been reached. Given that the increment of the relevant instability vanishes at $I = I_0$ [43], one can expect that the switching occurs in a monotonic way.

In summary, quasi-stationary transitions between states with different symmetries are related to symmetry-breaking (pitchfork) bifurcations of steady-state solutions; abrupt transitions are related to bifurcations of steady-state solutions provided that they occur in a monotonic way, i.e., without temporal oscillations, and the relevant bifurcations are pitchfork or fold.

Discharge vessels are axially symmetric in many experiments. Pitchfork bifurcations of only two types may occur in such configurations [43, 63]. First, it is breaking

of axial symmetry, i.e., branching of a 3D mode, where the distribution of luminosity over the electrode surface is periodic in the azimuthal angle with an arbitrary period (2π, or π, or $2\pi/3$, or $\pi/2$ *etc*), from a 2D mode, where the distribution of luminosity is axially symmetric. Second, it is doubling of period with respect to the azimuthal angle, i.e., branching from a 3D mode with one of the periods π, $\pi/2$, $\pi/3$, $\pi/4$ *etc* of a 3D mode with double this period. It follows, in particular, that transitions with changes of symmetry of other types cannot occur through pitchfork bifurcations of steady-state solutions, and are always abrupt.

The above general reasoning is valid for mode changes on electrodes of any dc discharges. In the next sections, this reasoning will be applied to particular cases of cathodes of arc and dc glow discharges.

4.3 Mode transitions on cathodes of arc discharges

In the case of refractory cathodes of high-pressure arc discharges, the theory based on the concept of multiple solutions has gone through a detailed experimental validation by means of different methods, such as spectroscopic measurements, electrostatic probe measurements, electrical and pyrometric measurements, and calorimetry; see, e.g., [37, 94–96], review [97] and references therein, and also the recent review [98]

The theory of current transfer to cathodes of arc discharges is simpler from the theoretical point of view than the theory for the case of glow discharge. The eigenvalue problem governing the stability of steady-state solutions against small perturbations is self-adjoint (Hermitian) in this case [39]. This means, in particular, that the spectrum of perturbations is real, a conclusion that was confirmed by numerical calculations [38, 99]. It follows that all abrupt transitions are monotonic in time. Indeed, no oscillations of arc voltage and luminosity of the cathode surface is observed in the experiments on transitions between diffuse and spot modes on arc cathodes; e.g., [95, 100–102]. Hence, all abrupt transitions are related to bifurcations of steady-state solutions. In more general terms, any transition between different modes, be it quasi-stationary or abrupt, is related to bifurcations of steady-state solutions in the case of arc cathodes.

In the simplest case of a rod cathode with a flat tip, a 2D diffuse mode of current transfer occurs in the experiment at high currents and a 3D mode with a spot at the edge of the cathode occurs at low currents, as schematically shown by solid lines in Figure 4.1. (Note that patterns with several spots have been observed on cathodes of high-pressure arc discharges in more complex arrangements, such as magnetically rotating arcs [103].) The transitions between the two modes are shown by the arrows in Figure 4.1; they are abrupt without temporal oscillations and manifest hysteresis.

In agreement with the reasoning of Sec. 4.2, these transitions represent an indication of the presence of pitchfork or fold bifurcations of steady-state solutions.

The latter conclusion may be compared with theoretical results [38, 39]. The theory predicts that the diffuse mode and the 3D mode with a spot at the edge of the cathode are the only modes that contain stable sections. The stable and unstable sections of each mode are schematically shown in Figure 3.1. In the case of the diffuse mode, these sections are separated by the state B, where a subcritical pitchfork bifurcation occurs. In the case of the spot mode, the stable and unstable sections are separated by the turning point K, where a fold bifurcation occurs. Thus, the accurate theory indicates that the transition from the diffuse mode to the spot mode is related to the pitchfork bifurcation and the return transition is related to the fold bifurcation, in agreement with the reasoning of Sec. 4.2.

4.4 Mode transitions on cathodes of dc glow discharges

4.4.1 State-of-the-art of the theory

In the case of dc glow discharges, multiple solutions have been shown to exist even in the most basic models and the solutions computed up to now describe many features of the patterns observed; e.g., [63] and references therein and [104]. In particular, the modelling has shown that self-organization on cathodes of glow microdischarges can occur not only in xenon, but also in other plasma-producing gases; a prediction which has been confirmed by subsequent observations of microdischarges in krypton [53] and argon [105]. On the other hand, the comparison between the theory and the experiment has been merely qualitative up to now.

The eigenvalue problem governing stability of steady-state solutions against small perturbations is not self-adjoint for glow cathodes. Therefore, the spectrum of perturbations need not be real. Indeed, a numerical investigation of stability of 2D modes [106] has given a spectrum that contains both real and complex eigenvalues (and is considerably more elaborate than the spectrum in the case of arc cathodes). It follows that abrupt transitions between different spot patterns may be oscillatory, in contrast to the case of arc cathodes. Note that this conclusion is consistent with the experiment: for example, temporal oscillations of the discharge voltage have been observed in the course of transition from the Townsend to normal discharge [107–109].) Such transitions are unrelated to bifurcations of steady-state solutions.

4.4.2 Analyzing experimental observations

A wealth of self-organized spot patterns and transitions between different patterns has been observed on cathodes of dc glow microdischarges [7, 46–54, 110, 111]. It follows from Sec. 4.2 that a detailed experimental investigation of transitions between different spot patterns, performed with sufficiently small steps in I and a sufficiently high temporal resolution, is needed to unambiguously identify transitions that are related to bifurcations of steady-state solutions. Unfortunately, such investigations seem to be absent. The most detailed data are published in the work [54], where the discharge current was adjusted on the microampere scale. The question as to whether the observed transitions are quasi-stationary or abrupt with or without oscillations was not studied. However, transitions between states of different symmetries that seem to be continuous (i.e., quasi-stationary) have been observed; e.g., transitions between states with a large spot occupying the central part of the cathode and a ring-like arrangement of four spots [54, Fig. 2], or between a ring spot and a ring-like arrangement of five spots [54, Fig. 5]. Question arises as to if these transitions can occur through pitchfork bifurcations of steady-state solutions, according to the first scenario described in Sec. 4.2.

In more general terms, one can try to identify in the observations [7, 46–54, 110, 111] all changes of symmetry that may occur through pitchfork bifurcations of steady-state solutions. There is a possibility that these transitions can be realized in a quasi-stationary way, although this is not always the case as exemplified by the transition depicted by the vertical arrow above state B in Fig. 1. On the contrary, transitions that are unrelated to pitchfork bifurcations of steady-state solutions surely cannot be realized in a quasi-stationary way, i.e., are always abrupt.

The discharge vessels are axially symmetric in most of the above-cited experiments. If follows from Sec. 4.2 that pitchfork bifurcations of only two types may occur in such configurations: breaking of axial symmetry and doubling of period with respect to the azimuthal angle. Hence, one should try to identify transitions with changes of symmetry of these two types in the available experimental data [7, 46–54, 110, 111]. If such transitions exist, one should try to find the relevant bifurcations by means of numerical modelling. If the bifurcations have been found, one will be able to compare the computed patterns in the vicinity of the bifurcation points with the patterns observed in the experiments.

Most of the transitions reported in [7, 46–54, 110, 111] do not belong to either of the two above types. None of these transitions can occur through bifurcations of steady-state solutions, hence these transitions cannot be realized in a quasi-stationary way. In particular, this applies to successive transitions between ring arrangements of

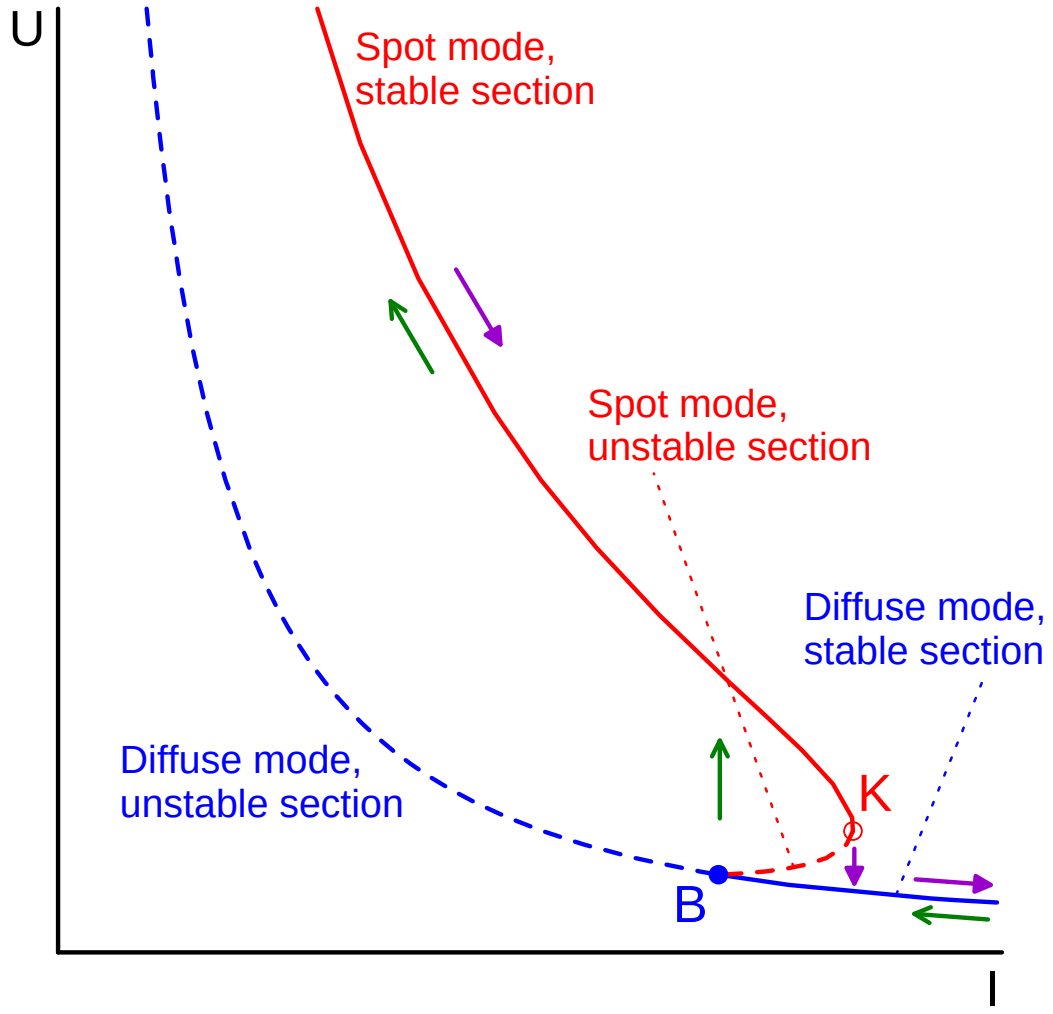

Figure 4.1: Schematic of current-voltage characteristics (CVCs) of the diffuse mode of current transfer to rod cathodes of high-pressure arc discharges and of the mode with a spot at the edge of the cathode. The sections shown by the solid lines and the transitions shown by the arrows are observed in the experiment.

4, 5, 6, 5, 4, and 3 spots shown in, e.g., [54, Fig. 2] and [48, Fig. 2]. It is interesting to point out that this conclusion is consistent with the experimental observation that the transition between the ring arrangements of 6, 5, and 4 spots was irreversible: it could be realized when the current is lowered, but attempts to increase the current, when the discharge was operating in these modes, led to the extinction of the discharge [48].

However, transitions that do belong to one of the two possible types of pitchfork bifurcation (with either a breaking of axial symmetry, or a doubling of period with respect to the azimuthal angle) have been observed and are listed in Table 4.1. Note that the two aforementioned transitions observed in [54] that appear to be quasi-stationary (those between states with a large spot occupying the central part of the cathode and a ring-like arrangement of four spots [54, Fig. 2] and between a ring spot and a ring-like arrangement of five spots [54, Fig. 5]) exhibit a breaking of axial symmetry and therefore can indeed occur through pitchfork bifurcations; accordingly, these transitions are listed in the table.

Higher-symmetry mode		Lower-symmetry mode		Source
Symmetry	Pattern	Symmetry	Pattern	
2D	Central spot	3D, π	2 symmetric spots	[48, Fig. 5]
2D	Central spot	3D, $\pi/2$	Ring of 4 spots	[48, Fig. 2], [54, Fig. 2]
2D	Ring spot	3D, $2\pi/5$	Ring of 5 spots	[54, Fig. 5]
2D	Central spot, ring spot	3D, $2\pi/5$	Central spot, ring of 5 spots	[54, Fig. 6]
3D, $\pi/3$	Ring of 6 spots	3D, $2\pi/3$	2 rings of 3 spots each	[112]

Table 4.1. Transitions between modes with different spot patterns observed on cathodes of glow microdischarges that are potentially related to bifurcations. Numbers in the columns 'Symmetry' in cases of 3D modes designate azimuthal period.

The bifurcation that can be responsible for the second transition in Table 4.1 was encountered in [104]. The period-doubling bifurcation that can be responsible for the fifth transition has been encountered as well, although for plasma-producing gases different from xenon, which was used in the experiments [112]: helium [57, Fig. 9] and krypton [53, Fig. 2]. In this work, these bifurcations are numerically investigated in detail and the computed patterns in the vicinity of the bifurcation points are compared with the experiment. Also reported in this work is the finding and analysis of the bifurcation that corresponds to the third transition in Table 4.1,

for which experimental images taken with a very fine step over discharge current are available [54, Fig. 5].

4.4.3 Numerical modelling

The models

Two numerical models of glow discharges are used in this work, one of them being basic and the other one more detailed. Both models follow standard lines. For completeness, a summary of differential equations, boundary conditions, and data used for transport and kinetic coefficients is given in Appendix 4.5. In brief, the models may be described as follows.

The detailed model comprises equations of conservation of electrons, singly charged atomic ions, singly charged molecular ions, excimers, and an effective species for excited atoms that combines all of the excited states of the $6s$ manifold ($6s[3/2]_2$, $6s[3/2]_1$, $6s'[1/2]_0$, and $6s'[1/2]_1$), Poisson's equation, and an equation for the conservation of electron energy. Transport equations for charged-particle species and electron energy density are written in the drift-diffusion approximation, transport equations for the excited neutral species describe diffusion. The geometry considered is that of the so-called cathode boundary layer discharge device, which was used in the vast majority of the experiments [7, 46–54, 110, 111] and comprises a flat cathode and a perforated anode, separated by a dielectric, with the radius of the opening in the anode equal to the radius of the discharge cavity in the dielectric; e.g., Figure 1 of [54]. It is assumed that the charged and excited particles coming from the plasma are absorbed, and subsequently neutralized and deexcited, respectively, at the surfaces of the electrodes and the dielectric.

The above-described detailed model is computationally costly and therefore not suitable for serial 3D simulations, required for the purposes of this work. It was shown previously experimentally [49] and computationally [104] that self-organized patterns in the cathode boundary layer discharge and a discharge with parallel-plane electrode configuration are qualitatively similar. An account of detailed chemical kinetics does not produce a qualitative effect as well [57]. Therefore, most of simulations reported below have been performed by means of a more basic model, which relies on a simple chemical kinetic scheme and assumes a parallel-plane electrode configuration. (We note right now that the results obtained in the framework of the basic and detailed models are qualitatively similar, in agreement with the above.) The basic model takes into account only one ion species (molecular ions), the only ionization channel (direct ionization from the ground state by electron impact) with a rapid conversion of the produced atomic ions into molecular ions, and employs the local-field approximation

(i.e., the electron kinetic and transport coefficients are treated as known functions of the local reduced electric field). The discharge vessel is assumed to be a cylinder with the end faces being the electrodes and the lateral surface being insulating. The neutralization of the ions and the electrons at the dielectric is neglected, so particles coming from the plasma are reflected back. Note that the effect of the neutralization has been well understood by now (e.g., [104] and references therein); as far as 3D spots are concerned, it results in the migration of spots away from the wall in the direction to the center of the cathode [57]. With this in mind, the assumption of negligible neutralization is sufficient for most purposes of this work, while making computations less costly and easier to analyze.

Identifying the relevant bifurcations

Results of simulations reported in this section have been obtained by means of the basic model for the following conditions: a discharge in xenon under the pressure of 30 Torr, the electron temperature $T_e = 1\,\mathrm{eV}$, the heavy-particle temperature $T_h = 300\,\mathrm{K}$, the interelectrode gap and discharge radius both of 0.5 mm, and the secondary electron emission coefficient $\gamma = 0.03$.

In order to show the place of the bifurcations being investigated (those corresponding to the second, third, and fifth transitions in Table 4.1) in the general pattern of self-organization in dc glow microdischarges, we will briefly introduce the latter, referring to [63] for details. In the framework of the basic model, the problem admits a 1D solution describing a mode in which all the variables depend only on the axial variable. This mode exists at all values of the discharge current and may be termed the fundamental mode. There are also multidimensional modes which bifurcate from, and rejoin, the fundamental mode; the so-called second-generation modes. Figure 4.2 depicts the current-voltage characteristics (CVC) of the fundamental mode and the first five second-generation modes. $\langle j \rangle$ in this figure is the average current density evaluated over a cross section of the discharge vessel (which is proportional to the discharge current). The schematics illustrate distributions of current density on the cathode surface associated with each mode. a_i and b_i designate bifurcation points where second-generation modes branch off from and rejoin the fundamental mode. The modes are ordered by decreasing separation of the bifurcation points: the mode designated a_1b_1 and is the one with the bifurcation points positioned further apart, the mode a_2b_2 is the one with the second largest separation between bifurcation points, and so on.

The modes a_1b_1 and a_3b_3 have been computed previously ([42] and [56], respectively) and are included in Figure 4.2 for the sake of completeness; we only note that

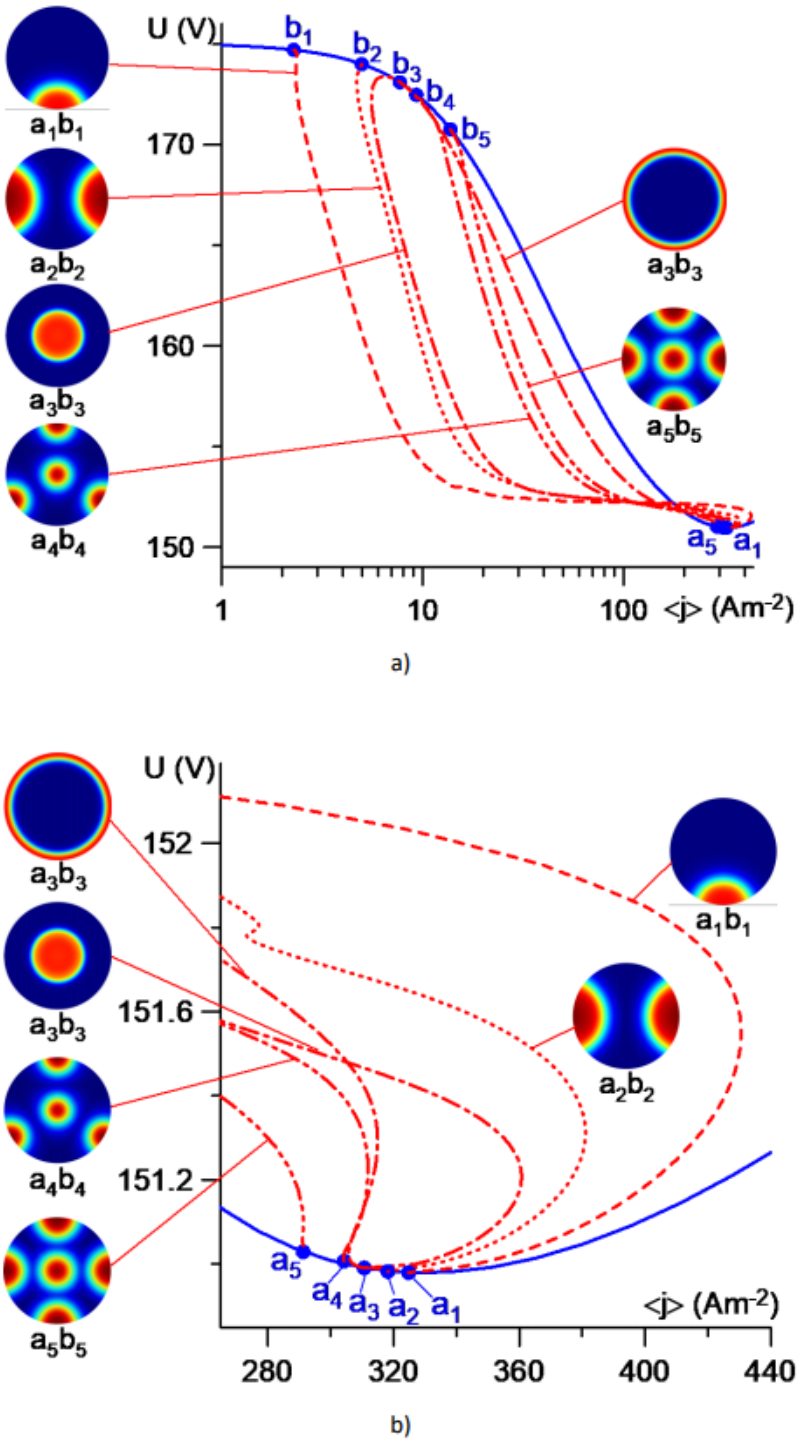

Figure 4.2: CVCs. Solid: the 1D (fundamental) mode. Dashed-dotted: 2D mode a_3b_3. Other lines: different 3D modes. Circles: bifurcation points. Top: General view. Bottom: Details near the point of minimum of the CVC of the 1D mode.

a_1b_1 is 3D with the azimuthal period of 2π while a_3b_3 is 2D with one branch associated with a spot at the center of the cathode and the other branch with a ring spot at the periphery of the cathode. The other modes, a_2b_2, a_4b_4, and a_5b_5, are 3D with periods π, $2\pi/3$, and $\pi/2$, respectively. The evolution with discharge current of the cathodic spot patterns associated with these modes is shown in Figure 4.3. Let us consider first the evolution of the patterns associated with the mode a_2b_2; Figure 4.2(a). The state 151.05 V is positioned in the vicinity of the bifurcation point a_2 and the spot pattern comprises two very diffuse cold spots at the periphery of the cathode. Further away from a_2, the cold spots expand and at state 151.79 V start merging. This corresponds to the retrograde section of the CVC a_2b_2 seen in Figure 4.2(b) in a narrow current range around 280 A m^{-2}. As current is further reduced towards b_2, the two cold spots expand further and the resulting pattern comprises two well-pronounced hot spots at the periphery; state 160.4 V. Note that this pattern is similar to those observed in the experiment; cf. [48, Fig. 5]. Finally, the state 173.93 V is positioned in the vicinity of the bifurcation point b_2 and the hot spots are very diffuse.

The patterns associated with the mode a_4b_4 are shown in Figure 4.3(b). The state 151.01 V is positioned in the vicinity of the bifurcation point a_4 and the pattern comprises three very diffuse cold spots at the periphery. Further away from a_4, the spots become better pronounced and a cold spot appears at the center; states 151.15 V and 151.53 V. Note that similar patterns with three hot spots have been observed in the experiment, cf. [48, Fig. 5] and [54, Fig. 2]. As current is further reduced towards b_4, the cold spot at the center is gradually transformed into a hot spot. The hot spots become well pronounced and a pattern comprising three (hot) spots at the periphery and a central spot is formed; state 151.74 V. (It is this pattern which is shown in the schematic in Figure 4.1) Note that patterns with three spots at the periphery and a spot at the center similar to that of the state 151.74 V have also been observed in the experiment, cf. [52, Fig. 4]. Note also that the transition between patterns with well-defined cold and hot spots is not accompanied by retrograde behavior, in contrast with the case of the mode a_2b_2. The state 172.48 V is positioned in the vicinity of the bifurcation point b_4 and the hot spots are very diffuse.

The evolution of patterns associated with the mode a_5b_5 shown in Figure 4.3(c) follows the same trend as the mode a_4b_4. Note that patterns with four spots at the periphery have also been observed in the experiment, cf. [48, Fig. 2], [54, Fig. 2].

A convenient graphical representation, or bifurcation diagram, of the modes a_4b_4 and a_5b_5 is given in Figure 4.4 with the use of the coordinates $(\langle j \rangle, j_c)$, where j_c is the current density at the center of the cathode. This representation allows a quick identification of the state where the switching between patterns comprising cold and hot spots at the center happens: it is the point in Figure 4.4 where the line

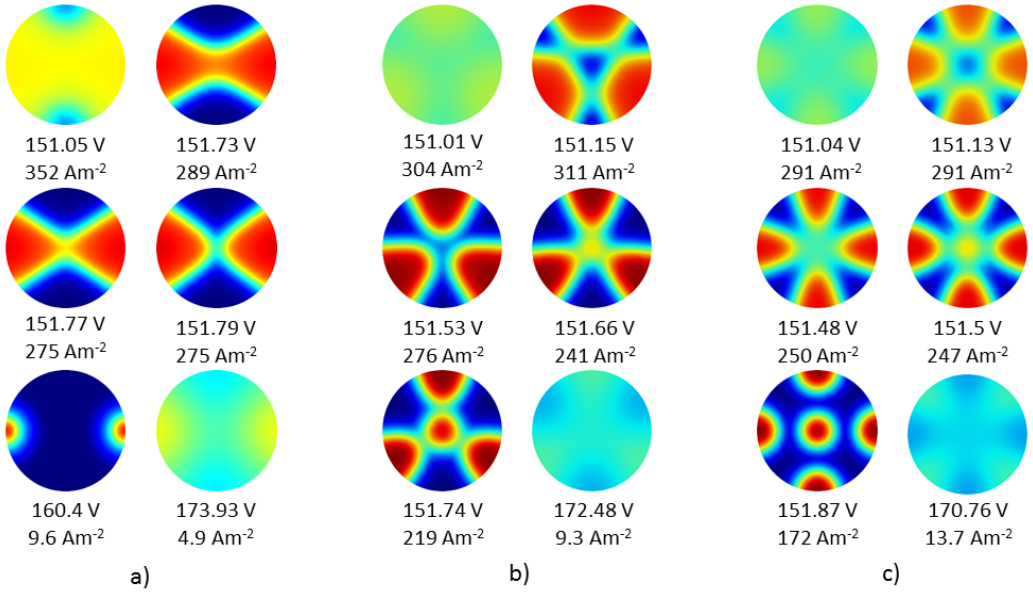

Figure 4.3: Evolution of distributions of current on the surface of the cathode associated with different modes. a): mode a_2b_2. b): a_4b_4. c): a_5b_5.

representing the mode in question intersects the straight line representing the 1D mode. For currents higher than the one corresponding to the switching, the current density at the center is lower than that corresponding to the 1D mode and the pattern comprises a cold spot at the center; $j_c > \langle j \rangle$ for lower currents and the pattern comprises a hot spot at the center.

Breaking of axial symmetry occurring at the state a_5 (Figures. 4.2 and 4.4) corresponds to the second transition in Table 4.1. In order to identify bifurcations corresponding to the third and fifth transitions, one needs to consider third-generation modes, i.e., 3D modes that branch off from and rejoin second-generation modes.

Three third-generation modes bifurcating from the mode a_3b_3, designated $a_{3,1}b_{3,1}$, $a_{3,2}b_{3,2}$, and $a_{3,3}b_{3,3}$, are shown in Figure 4.5. They branch off from and rejoin that branch of the mode a_3b_3 which is associated with a ring spot at the periphery; the bifurcations are breaking of axial symmetry. The modes $a_{3,1}b_{3,1}$, $a_{3,2}b_{3,2}$, and $a_{3,3}b_{3,3}$ have the periods of $2\pi/3$, $2\pi/5$, and $\pi/3$, respectively, and are associated with spot patterns comprising three spots at the periphery of the cathode, five spots, and six spots, respectively. Since none of the patterns shown in Figure 4.5 comprise a spot at the center, the coordinates $(\langle j \rangle, j_c)$ would be inconvenient and the coordinates $(\langle j \rangle, j_e)$ are used, where j_e is the current density at a fixed point on the periphery of the cathode which coincides with the center of one of the spots.

The evolution of the spot patterns associated with the mode $a_{3,2}b_{3,2}$ is shown in

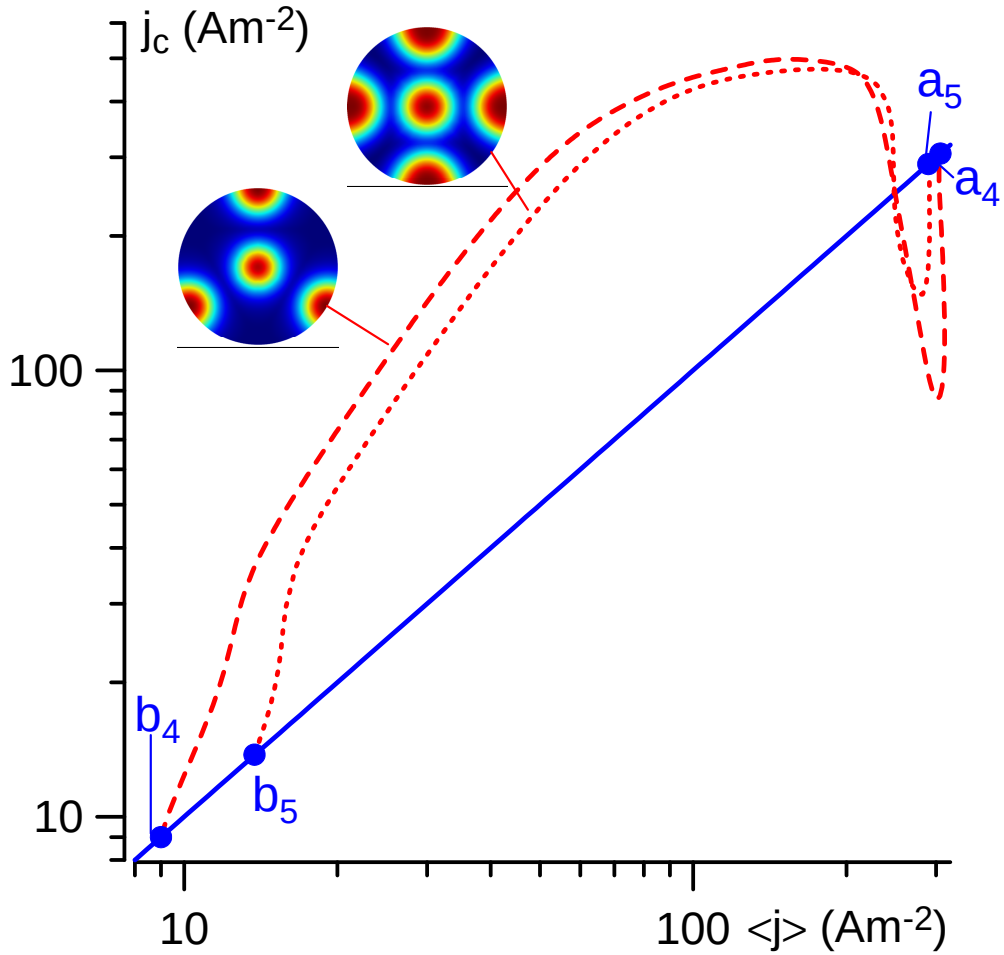

Figure 4.4: Bifurcation diagram. Solid: the 1D (fundamental) mode. Dashed, dotted: 3D second generation modes a_4b_4 and a_5b_5. Circles: bifurcation points.

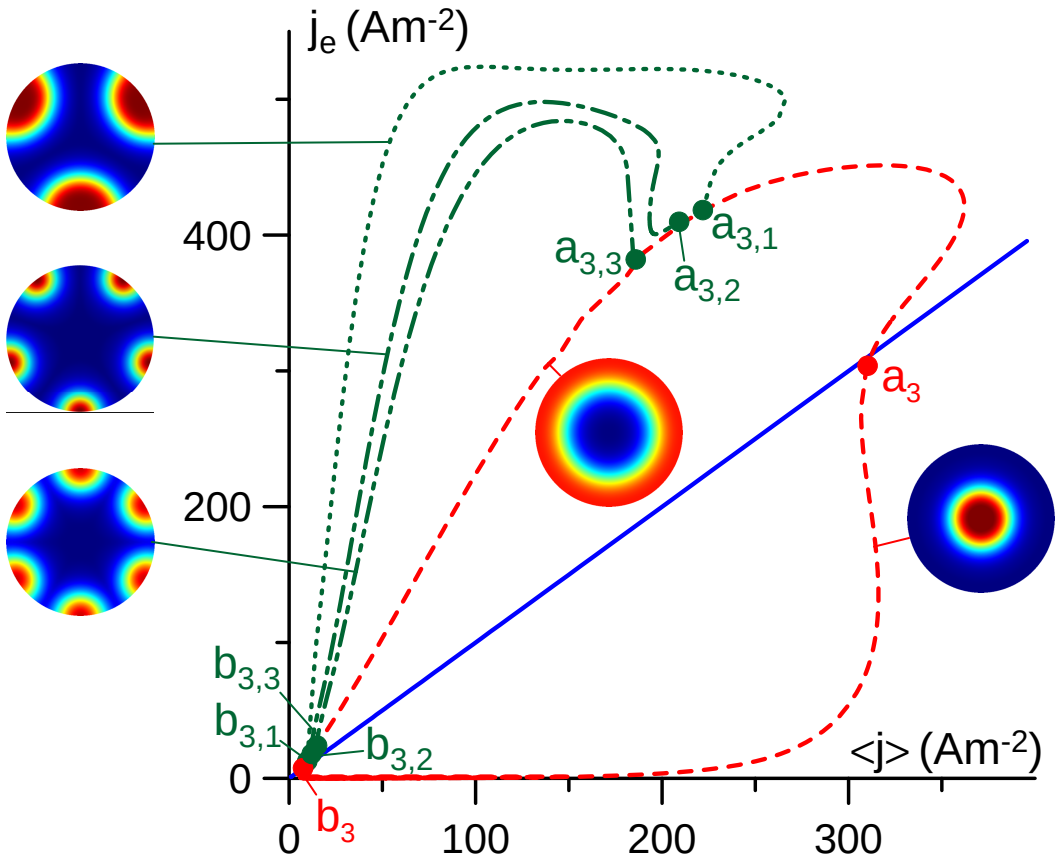

Figure 4.5: Bifurcation diagram. Solid: the 1D (fundamental) mode. Dashed: 2D mode a_3b_3. Other lines: 3D modes. Circles: bifurcation points.

Figure 4.6. At state 151.82 V, which is positioned near the bifurcation point $a_{3,2}$, the ring spot is slightly non-uniform in the azimuthal direction. Further away from $a_{3,2}$, the non-uniformity evolves into well-pronounced spots (states 151.81 V and 151.84 V). The spots become smaller as the current is further reduced (state 152.26 V). As the bifurcation point $b_{3,2}$ is approached, the spots expand once again (state 167.94 V). In the close vicinity of $b_{3,2}$ (state 170.70 V) a ring spot with a weak non-uniformity in the azimuthal direction is seen. Note that patterns similar to those shown in Figure 4.6 have been observed in the experiment [54, Fig. 5].

The behavior of the modes $a_{3,1}b_{3,1}$ and $a_{3,3}b_{3,3}$ follows the same trend as the behavior of the mode $a_{3,2}b_{3,2}$. The patterns are similar to experimentally observed patterns comprising three and six spots inside the cathode; cf. [48, Figs. 2 and 5] and [54, Fig. 2]. Note, however, that the pattern with three spots associated with the mode $a_{3,1}b_{3,1}$

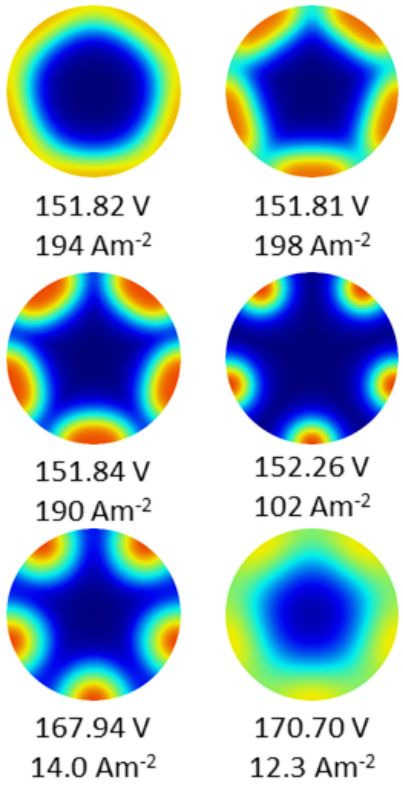

Figure 4.6: Evolution of distribution of current on the surface of the cathode associated with the mode $a_{3,2}b_{3,2}$.

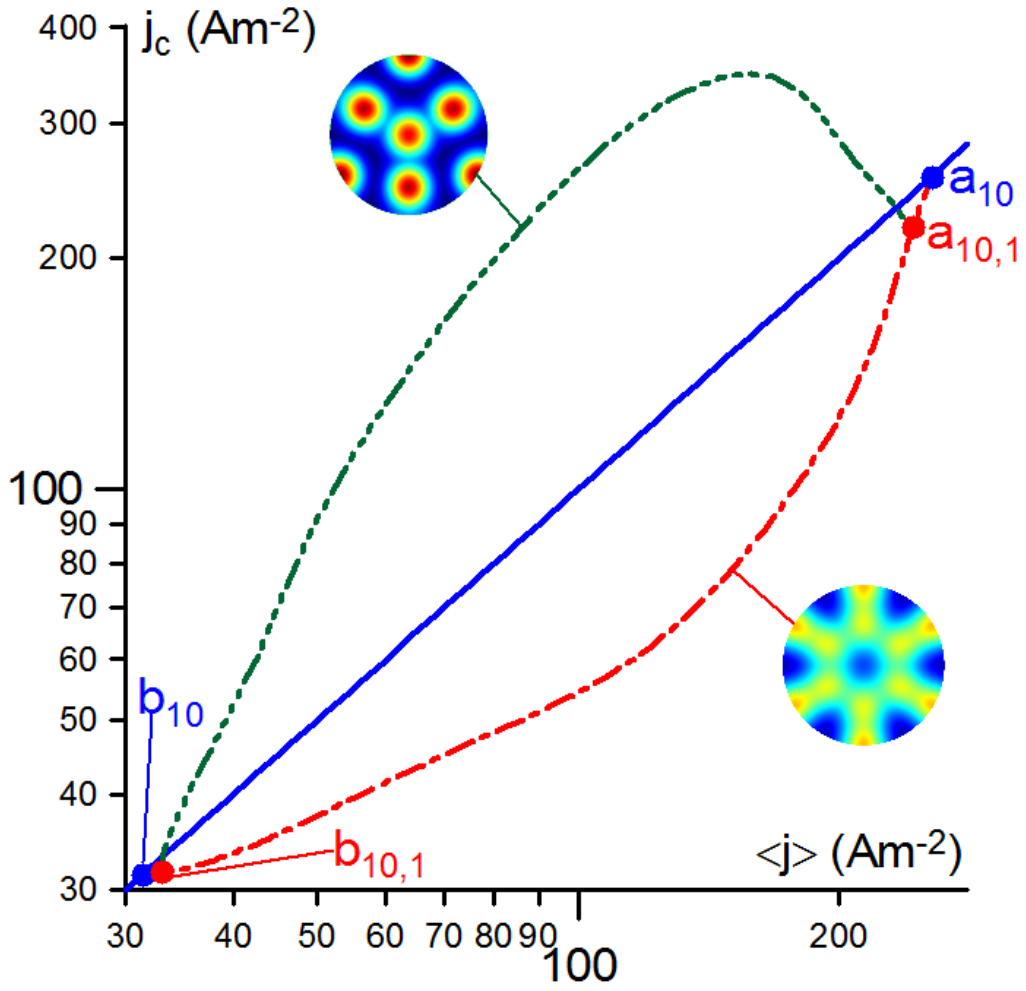

Figure 4.7: Bifurcation diagram. Solid: the 1D (fundamental) mode. Dashed: 3D second-generation mode $a_{10}b_{10}$. Dotted: 3D third-generation mode $a_{10,1}b_{10,1}$. Circles: bifurcation points.

is similar to the pattern with three spots appearing in some states belonging to a_4b_4 (states 151.15 V and 151.53 V in Figure 4.3(b)) and it is difficult to know which one of these two modes was observed in the experiments [48, 54]. A similar comment applies to the mode $a_{3,3}b_{3,3}$.

Breaking of axial symmetry occurring at the states $a_{3,2}$ and $b_{3,2}$ in Figure 4.5 corresponds to the third transition in Table 4.1. The bifurcation corresponding to the fifth transition is period doubling occurring at the state $a_{10,1}$ in Figure 4.7. Here $a_{10}b_{10}$ is a second-generation mode with the period of $\pi/3$ and $a_{10,1}b_{10,1}$ is a third-generation mode with the period of $2\pi/3$. The period doubling at $a_{10,1}$ occurs as follows: every second spot gradually moves from the periphery towards the center of the cathode; eventually a central spot is formed. (Note that the image illustrating the

mode $a_{10,1}b_{10,1}$ in Figure 4.7 corresponds to the situation where the central spot has already been formed.) This is similar to how the similar bifurcation occurs in helium [57, Fig. 9] and krypton [53, Fig. 2] except that in krypton the central spot is already present at the bifurcation point $a_{10,1}$.

4.4.4 Comparing the modelling and the experiment

As discussed in the preceding section, the bifurcation corresponding to the second transition in Table 4.1 is breaking of axial symmetry occurring at the state a_5 (Figure 4.2 and 4.4), where a mode with a ring-like arrangement of four spots (mode a_5b_5) branches off from the (fundamental) mode with an axially symmetric spot occupying the whole cathode surface except for the periphery (the abnormal discharge). The bifurcation corresponding to the third transition is breaking of axial symmetry occurring at the states $a_{3,2}$ and $b_{3,2}$ (Figure 4.5), where a mode with a ring-like arrangement of five spots (mode $a_{3,2}b_{3,2}$) branches off from the axially symmetric mode with a ring spot (a_3b_3). The bifurcation corresponding to the fifth transition is period doubling occurring at the state $a_{10,1}$ (Figure 4.7), where the mode $a_{10,1}b_{10,1}$, which is associated with three spots at the periphery and three spots closer to the center and has the period of $2\pi/3$, branches off from the mode $a_{10}b_{10}$, which is associated with a ring-like arrangement of 6 identical spots at the periphery and has the period of $\pi/3$.

The computed patterns in the vicinity of the bifurcation points are compared with the patterns observed in the experiments in Figure 4.8. The experimental images shown in Figure 4.8(a) and 4.8(b) have been taken from Figure 2 and 5, respectively, of [54]. Those shown in Figure 4.8(c) have been kindly provided by W. Zhu and P. Niraula [112]; we note for completeness that the geometry in this experiment was the same as in [54], the Xe pressure was 100 torr, and the current and voltage were nearly the same for both frames: 0.155 mA and 278 V.

The first one of the computed images shown in Figure 4.8(a) represents the bifurcation point a_5. The other images correspond to states belonging to the mode a_5b_5 in the vicinity of a_5. The last one of the computed images shown in Figure 4.8(b) represents the bifurcation point $a_{3,2}$, the other images correspond to states belonging to the mode $a_{3,2}b_{3,2}$ in the vicinity of $a_{3,2}$. The first one of the computed images shown in Figure 4.8(c) represents the bifurcation point $a_{10,1}$, the other images correspond to states belonging to the mode $a_{10,1}b_{10,1}$ in the vicinity of $a_{10,1}$.

It is seen from Figure 4.8 that the computed patterns in the vicinity of the bifurcation points closely resemble the patterns observed in the experiments. This supports the hypothesis that the transitions between patterns of different symmetries observed in the experiment and listed in the second, third, and fifth lines of Table 4.1 are

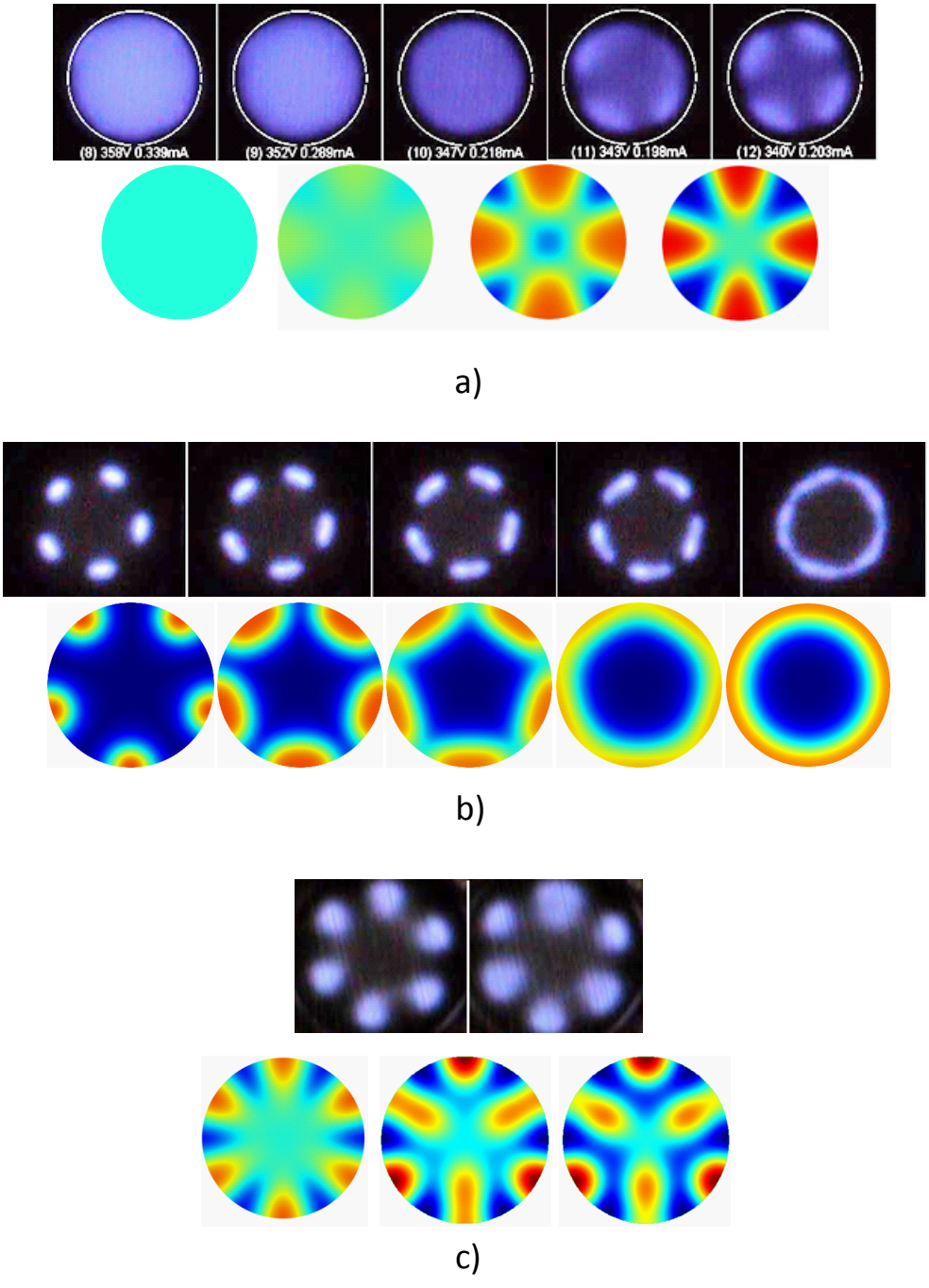

Figure 4.8: Experimentally observed and computed transitions between different modes in xenon.

quasi-stationary and occur through pitchfork bifurcations.

The transition between the abnormal discharge and a mode with four spots, shown in Figure 4.8(a), resembles the well-known transition between the abnormal and normal glow discharges, the difference being that there are four spots in the 3D mode and not just one as in the normal discharge. A question arises as to what is the reason of this difference and why just four spots are formed and not two or three. This question is related to a more general question as to why patterns with multiple spots have been observed in glow microdischarges but not in regular-scale glows and is of significant interest.

It is seen from Figure 4.2 that the mode with four spots at the periphery branches off from the abnormal discharge, at the state a_5, through a supercritical bifurcation, while the modes with one, two, and three spots branch off, at the states a_1, a_2, and a_4, through subcritical bifurcations. (Note that this is a typical situation: low- and high-order second-generation modes tend to branch off through, respectively, subcritical and supercritical bifurcations [63, Fig. 3].) As discussed in Sec. 4.2, a usual necessary condition for a quasi-stationary transition between two steady-state modes connected by a pitchfork bifurcation is that the bifurcation be supercritical. Therefore, it may seem that the modelling results shown in Figure 4.2 explain why the abnormal discharge in the experiment with microdischarges goes into the mode with four (rather than one, two, or three) spots, as seen in Figure 4.8(a). On the other hand, the experimental CVC of this transition [54, Fig. 3a] apparently represents a diagram of a subcritical bifurcation, and so does also the CVC shown in [48, Fig. 3a]. Thus, there is a discrepancy between the measurements, on one hand, and numerical modelling and the usual trend of the bifurcation theory, on the other. The other discrepancy between the measured and computed CVCs is that the discharge voltage in the 3D mode is lower than that in the (axially symmetric) abnormal mode in the experiment but slightly higher in the modelling.

In order to try to resolve the discrepancies, the bifurcations occurring at the states a_4 and a_5 have been recomputed by means of the detailed model, described in Sec. 4.4.3 and Appendix **??**; Figure 4.9. Since the geometry of the discharge vessel and the boundary conditions describing absorption of the charged particles at the wall invalidate the 1D solution, the role of the fundamental mode (abnormal discharge) is played by the first 2D mode [63]. All second-generation solutions are 3D, and the first four modes, which have the periods of 2π, π, $2\pi/3$, and $\pi/2$, respectively, are designated a_1b_1, a_2b_2, a_4b_4, and a_5b_5 (i.e., the designation a_3b_3 is skipped in order to maintain consistency with the designations of the second-generation modes computed in the framework of the basic model).

It is seen from the schematics in Figure 4.9 that the account of neutralization of

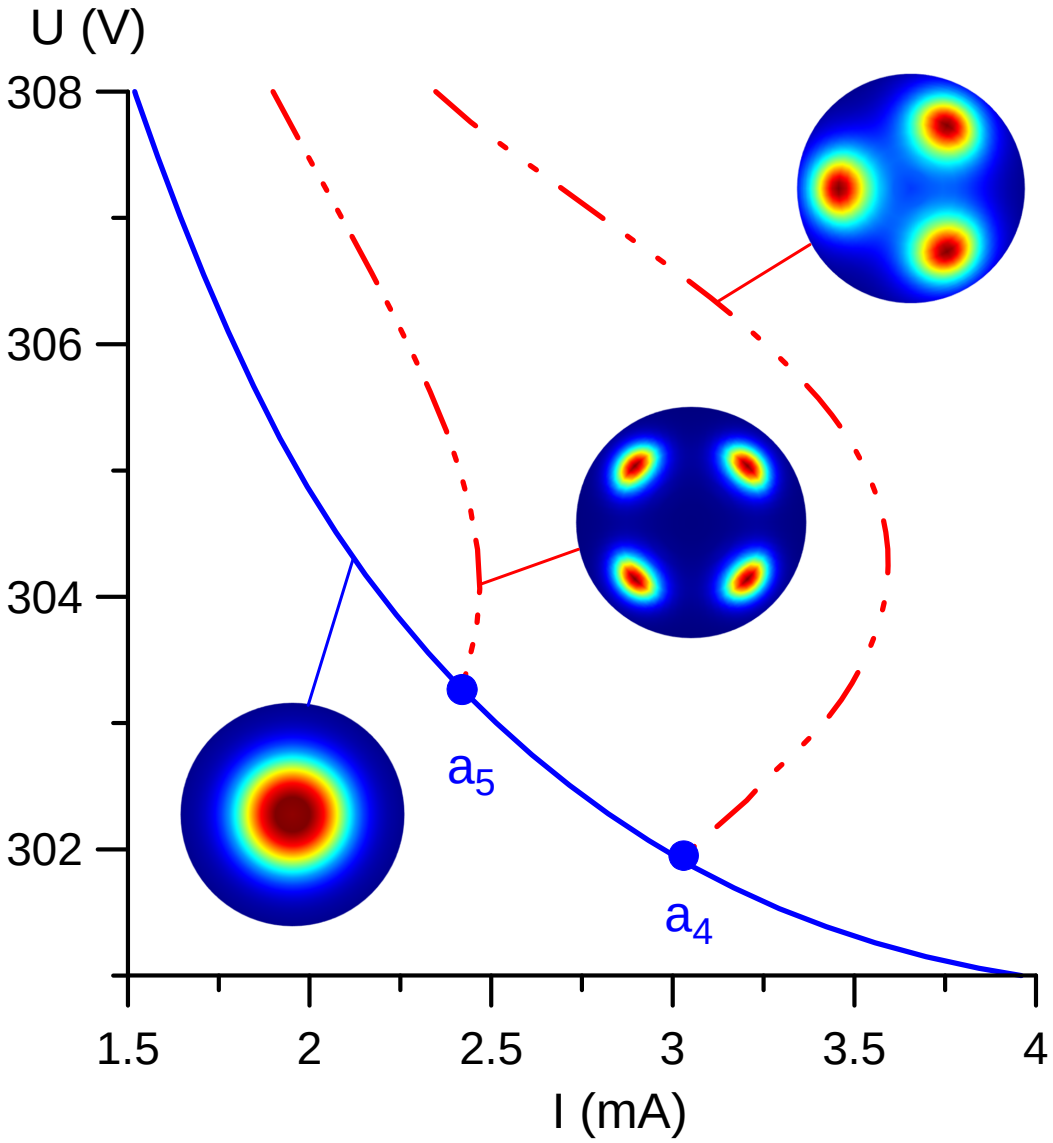

Figure 4.9: CVCs. Detailed model. Solid: the first 2D (the fundamental) mode. Other lines: 3D modes a_4b_4 and a_5b_5. Circles: bifurcation points.

the charged particles at the wall of the vessel causes the spots to migrate from the edge to the inside of the cathode. The discharge voltage computed in the framework of the detailed model is significantly higher than the voltage in the basic model. On the other hand, the patterns of the CVCs are similar, in agreement with what was said in Sec. 4.4.3. In particular, the bifurcation occurring at a_5 is supercritical while the one at a_4 is subcritical (as well as those at a_1 and a_2, which are not shown in Figure 4.9) and the discharge voltage in the 3D modes in both models is slightly higher than that in the fundamental mode. Thus, the above-described discrepancies have not been resolved and further computational and experimental work is needed.

4.5 Summary and the work ahead

The existence, or not, of bifurcations of steady-state solutions describing different modes of current transfer to electrodes of dc discharges is related to the underlying physics and is therefore of significant interest. Bifurcations manifest themselves in the experiment as transitions between modes with different spot patterns, which occur as the discharge current I is varied. Two scenarios of such transitions are possible: (1) quasi-stationary (continuous) and, consequently, reversible transitions between states where distributions of luminosity over the electrode surface possess different symmetries and (2) transitions that occur abruptly even for very small variations of I. Quasi-stationary transitions are related to a symmetry-breaking (pitchfork) bifurcation. If the discharge vessel is axially symmetric, pitchfork bifurcations of only two types may occur: breaking of axial symmetry and doubling of period with respect to the azimuthal angle. Abrupt transitions that occur in a monotonic way, i.e., without temporal oscillations, are related to pitchfork or fold bifurcations. Finally, abrupt transitions accompanied by temporal oscillations are unrelated to a bifurcation of steady-state solutions.

The above general reasoning is valid for mode changes on electrodes of any dc discharges. In the case of (refractory) cathodes of high-pressure arc discharges, the eigenvalue problem governing stability of steady-state solutions against small perturbations is self-adjoint and its spectrum is real. Therefore, all abrupt transitions are monotonic in time, in agreement with what is known from the experiment. It follows that any transition between different modes, be it quasi-stationary or abrupt, is related to a bifurcation of steady-state solutions in the case of arc cathodes. Thus, transitions between diffuse and spot modes of current transfer, frequently observed in the experiment, represent an indication of the presence of pitchfork or fold bifurcations of steady-state solutions, as predicted by the theory.

A wealth of spot patterns and transitions between different patterns have been

observed on cathodes of dc glow microdischarges [7, 46–54, 110, 111]. In particular, transitions between states of different symmetries that seem to be continuous (i.e., quasi-stationary) have been observed in [54]. It is legitimate to hypothesize that such transitions occur through pitchfork bifurcations (breaking of axial symmetry or period doubling) of steady-state solutions according to the first above-mentioned scenario. This hypothesis has been confirmed by numerical modelling: the relevant bifurcations have been found and the computed patterns in the vicinity of the bifurcation points are found to closely resemble the patterns observed in the course of the transitions in the experiment. Note that new 3D modes of current transfer were computed in the course of finding the bifurcations and these new modes are associated with experimental spot patterns reported in the literature.

Thus, available experimental data on multiple modes of current transfer to cathodes of dc glow and arc discharges provide clear indications of the presence of pitchfork or fold bifurcations of steady-state solutions, as predicted by the theory. While the comparison between the theory and the experiment still remains qualitative in the case of dc glow cathodes, the agreement is convincing and lends further support to the theory.

A detailed experimental investigation of transitions between different spot patterns on cathodes of glow microdischarges, performed with sufficiently small steps in I and a sufficiently high temporal resolution and accompanied by numerical modelling, would allow verification of the above scenarios. For example, it would be very interesting to verify the theoretical prediction that successive transitions between ring arrangements of 4, 5, 6, 5, 4, and 3 spots shown in, e.g., [54, Fig. 2] and [48, Fig. 2] cannot be realized in a quasi-stationary way, in contrast to the second, third, and fifth transitions in Table 4.1. It should be stressed that this prediction is consistent with the experimental observation that the transition between the ring arrangements of 6, 5, and 4 spots was irreversible [48]. Note also that the theory predicts that any transition, except those between an axially symmetric mode and a 3D mode and those between 3D modes with doubling of azimuthal period, will be abrupt even for very small variations of discharge current and/or voltage.

Another interesting question to be addressed is the one discussed in the end of Sec. 4.4.4 and concerns the discrepancy between the measured CVC of the transition from the abnormal discharge and the mode with four spots, on the one hand, and numerical modelling as well as the usual trend of the bifurcation theory, on the other.

Appendix: Equations and boundary used in chapter 3

The system of differential equations describing the detailed model reads

$$\begin{aligned}
\nabla\cdot\mathbf{J}_e &= S_e, \quad \mathbf{J}_e = -D_e\,\nabla n_e + n_e\,\mu_e\,\nabla\varphi;\\
\nabla\cdot\mathbf{J}_\varepsilon &= e\mathbf{J}_e\cdot\nabla\varphi - S_\varepsilon, \quad \mathbf{J}_\varepsilon = -D_\varepsilon\,\nabla n_\varepsilon + n_\varepsilon\,\mu_\varepsilon\,\nabla\varphi;\\
\nabla\cdot\mathbf{J}_{i\beta} &= S_{i\beta}, \ \mathbf{J}_{i\beta} = -D_{i\beta}\,\nabla n_{i\beta} - n_{i\beta}\,\mu_{i\beta}\,\nabla\varphi;\\
\nabla\cdot\mathbf{J}_{ex\beta} &= S_{ex\beta}, \quad \mathbf{J}_{ex\beta} = -D_{ex\beta}\,\nabla n_{ex\beta};\\
\varepsilon_0\,\nabla^2\varphi &= -e\,(n_{i1} + n_{i2} - n_e).
\end{aligned} \tag{4.1}$$

Here $\beta = 1, 2$; the indexes $e, \varepsilon, i1, i2, ex1, ex2$ refer to electrons, electron energy density, atomic ions, molecular ions, atoms in excited states, and excimers, respectively; n_α, $\mathbf{J}_\alpha$, D_α, μ_α, S_α are the number density, density of the transport flux, diffusion coefficient, mobility, and rate of production of particles per unit time and unit volume of species α ($\alpha = e, i1, i2, ex1, ex2$); the electron energy density is defined as $n_\varepsilon = n_e\overline{\varepsilon}$, where $\overline{\varepsilon}$ is the average electron energy, and coincides with 3/2 of the electron pressure; $\mathbf{J}_\varepsilon$ is the density of electron energy flux; D_ε and μ_ε are the so-called electron energy diffusion coefficient and mobility; S_ε is the rate of loss of electron energy per unit time and unit volume due to collisions; φ is electric potential; ε_0 is permittivity of free space, and e is the elementary charge. The transport coefficients used are the same as in [57]. The set of reactions comprises electron impact ionization from the ground state, an effective excited atomic state, and the metastable molecular state; excitation of atoms by electron impact; atomic ion conversion to molecular ions with neutral atoms playing the role of the third body; metastable pooling; dissociative recombination; photon emission from the atomic and molecular excited states; conversion of excited atoms to excimers with neutral atoms playing the role of the third body. The kinetic coefficients are the same as in [57].

The computation domain corresponds to the cathode boundary layer discharge device (e.g., Figure 1 of [54]). Let us introduce cylindrical coordinates (r, ϕ, z) with the origin at the center of the cathode and the z-axis coinciding with the axis of the vessel. Then the computation domain is a union of the cylinder $\{r < R,\ 0 < z < h_d + h_a\}$ and the half-space $\{z > h_d + h_a\}$, where h_d and h_a are thicknesses of the dielectric and the anode and R is the radius of the opening in the anode and of the cavity in the dielectric. The circle $\{r < R,\ z = 0\}$ is the surface of the cathode, $\{r = R,\ h_d < z < h_d + h_a\} \cup \{r > R,\ z = h_d + h_a\}$ is the surface of the anode, and the surface $\{r = R,\ 0 < z < h_d\}$ is dielectric.

The boundary conditions for Eqs. (4.1) are written in the conventional form (e.g.,

[113, 114]):

$$\begin{aligned}
J_{\alpha z} &= \frac{1}{4}\sqrt{\frac{8k_BT_\alpha}{\pi m_\alpha}}n_\alpha,\ J_{ez} = -\gamma J_{iz} - \gamma J_{i2z},\ J_{\varepsilon z} = (E_I - 2W)J_{ez},\ \varphi = 0\,; \\
J_{\alpha n} &= \frac{1}{4}\sqrt{\frac{8k_BT_\alpha}{\pi m_\alpha}}n_\alpha,\ J_{en} = \frac{1}{2}\sqrt{\frac{8k_eT_e}{\pi m_e}}n_e,\ J_{\varepsilon n} = \frac{1}{2}\sqrt{\frac{8k_BT_e}{\pi m_e}}n_\varepsilon,\ \varphi = U; \\
J_{\alpha r} &= \frac{1}{4}\sqrt{\frac{8k_BT_\alpha}{\pi m_\alpha}}n_\alpha,\ J_{er} = \frac{1}{2}\sqrt{\frac{8k_eT_e}{\pi m_e}}n_e,\ J_{\varepsilon r} = \frac{1}{2}\sqrt{\frac{8k_BT_e}{\pi m_e}}n_\varepsilon,\ J_{i1r} + J_{i2r} - J_{er} = 0,
\end{aligned} \tag{4.2}$$

at the surface of the cathode, anode, and dielectric, respectively. Here γ is the effective secondary emission coefficient, which is assumed to characterize all mechanisms of electron emission (due to ion, photon, and excited species bombardment) [2]; E_I is the ionization energy of the incident ions; W is the work function of the cathode surface; U is the discharge voltage; the subscripts r, z, and n denote radial, axial, and normal projections of corresponding vectors (the normal n points outwards from the computation domain); $\alpha = i1, i2, ex1, ex2$; k_B is Boltzmann's constant; $T_\alpha = T_h$, where T_h is the heavy-particle temperature (a given parameter); $T_e = 2\bar{\varepsilon}/3k_B$ is the electron temperature; and m_α are the particle masses.

Results of simulations performed by means of this model, reported in this work, refer to the following conditions: discharge in xenon under the pressure of 75 Torr, $T_h = 300\,\mathrm{K}$, $h_d = 0.25\,\mathrm{mm}$, $h_a = 0.25\,\mathrm{mm}$, $R = 0.375\,\mathrm{mm}$, and $\gamma = 0.075$.

The system of differential equations describing the basic model comprises the first and last equations in Eq. (4.1) and the third equation written for only one ion species. Boundary conditions at the cathode, anode, and dielectric are written as, respectively,

$$\begin{aligned}
z &= 0: \quad \frac{\partial n_i}{\partial z} = 0, \quad J_{ez} = -\gamma J_{iz}, \quad \varphi = 0\,; \\
z &= h: \quad n_i = 0, \quad \frac{\partial n_e}{\partial z} = 0\,, \quad \varphi = U; \\
r &= R: \quad \frac{\partial n_i}{\partial r} = \frac{\partial n_e}{\partial r} = 0\,, \quad J_{ir} - J_{er} = 0,
\end{aligned} \tag{4.3}$$

where n_i and $\mathbf{J}_i$ are the number density and transport flux density of the ions. The first boundary condition in the first line and the second boundary condition in the second line imply that diffusion fluxes of the attracted particles at the electrode surfaces are neglected compared to drift. The first and second boundary conditions in the third line imply that the neutralization of the ions and the electrons at the dielectric is neglected. The transport and kinetic coefficients used in the basic model for xenon are taken from [56].

Numerical results reported in this work have been computed using the commercial finite element software COMSOL Multiphysics. The detailed model was implemented using the Plasma module of COMSOL, which was adapted so that it could be used

in combination with a stationary solver and supplemented with a mesh element size based stabilization method to reduce the Péclet number. The basic model was implemented using the Transport of Diluted Species module, and also solved using a stationary solver.

Chapter 5

Conclusions of the thesis

In this work self-organized patterns of current density on electrodes of dc glow discharges were modelled. The modelling was performed in the framework of the fluid description of plasma.

Patterns of anodic spots were self-consistently computed in the conventional DC glow discharge model. The solution describing the spots was found in the same range of current as the spotless solution. The computed anode spots are similar to the spots on cathodes of arc and DC glow discharge in the following ways. Both are described by multiple steady state solutions and reveal azimuthal periodicity. The anoidc spots are different to the spots on cathodes of arc and DC glow discharge in the following ways. The solution describing the spotless mode for the anodes does not contain a pronounced N-shaped current-voltage characteristic; no bifurcations were found in a wide range of currents on the spotless mode, i.e., the anode spots were found to exist isolated from the 2D spotless mode. The anode spots are apparently related to the change in the sign of the near anode voltage. The electrode adjacent to the anodic spots behaves like a mini-cathode, in that the sign of the current density and electric field is reversed: the anode spots operate as a unipolar glow discharge.

In terms of cathodic spots, self-organized spots were computed in the cathode boundary layer discharge configuration. The form of the computed patterns is similar to those computed in the parallel-plane configuration and to those observed in the experiments in the sense that all of the spots comprise axially symmetric ring spots or circular arrangements of 3D spots. Activating a fully absorbing dielectric surface revealed spots not centered at the periphery of the cathode, but rather located inside the cathode, as they are in the experiment. A palindromic series of the number of spots with discharge current was found, which what is observed during the switching between modes with different patterns in the experiment [54].

In terms of current transfer to electrodes of DC discharges, a strong case was built

for the affirmative to the question of whether bifurcations of steady-state solutions exist or not on modes of current transfer to cathodes. For current transfer to cathodes of dc glow microdischarges, a wealth of spot patterns and transitions between different patterns have been observed in the experiments [7, 46–54, 110, 111],

transitions were found that are candidates for being manifestations of bifurcations. Numerical modelling was done to further evidence the candidates' cases of being bifurcations: relevant bifurcations were found and the computed patterns were found to closely resemble the patterns observed in the course of the transitions in the experiment. An analysis was made of transitions between different modes of current transfer to cathodes of arc discharges. Transitions between diffuse and spot modes of current transfer, frequently observed in the experiment, was found to represent an indication of the presence of pitchfork or fold bifurcations of steady-state solutions.

New 3D modes of current transfer to cathodes of glow discharges were computed, in framework of a basic model, in the course of finding the bifurcations, these new modes are associated with the experimental spot patterns reported in the literature. Modelling was performed in the experimental conditions, with a more detailed model that took into account multiple plasma and gas species, their chemistry, and using the local mean energy approximation. A discrepancy was found between the measured CVC of the transition from the abnormal discharge and the mode with four spots in the experiment on the one hand [54], and the detailed numerical modelling as well as the usual trends of the bifurcation theory on the other.

In future work, one may make a detailed experimental investigation of transitions between different spot patterns on cathodes of glow microdischarges, performed with sufficiently small steps in current and a sufficiently high temporal resolution, that would allow, for example, the verification of the prediction that successive transitions between ring arrangements of 4, 5, 6, 5, 4, and 3 spots shown in, e.g., [54, Fig. 2] and [48, Fig. 2] cannot be realized in a quasi-stationary way.

It would be of theoretical interest to investigate what effect the electric field dependence on secondary emission, e.g. as in [115], has on patterns of glow discharge spots. Also of theoretical interest is the question of why patterns with multiple spots have been observed on cathodes of glow microdischarges, but not in regular-scale glows.

The question of what the effect is on spots of liquid electrodes, as opposed to metallic ones, is of significant interest as it is spots on liquid anodes that are linked to a cancer inhibiting capacity [6].

Bibliography

[1] M. Faraday, Phil. Trans. **1**, p.125 (1838).

[2] Yu. P. Raizer, *Gas Discharge Physics* (Springer, Berlin, 1991).

[3] R. K. Marcus and J. A. C. Broekaert, *Glow Discharge Plasmas in Analytical Spectroscopy* (Wiley, 2003).

[4] D. Lee, H. Chung, and H. Kim, Rev. Sci. Instrum. (2000).

[5] H. R. Yousefi, M. Ghoranneviss, A. R. Tehrani, and S. Khamseh, Surf. Interface Anal. (2003).

[6] Z. Chen, S. Zhang, I. Levchenko, I. I. Beilis, and M. Keidar, Scientific Reports **7** (2017).

[7] K. H. Schoenbach and W. Zhu, IEEE J. Quantum. Electron. **48**, 768 (2012).

[8] A. von Engel, *Ionized gases* (Oxford University Press, 1965).

[9] M. Steenbeck, Physikalische Zeitschrift **XXXIII**, 809 (1932).

[10] Th. Peters, Z. Physik A **144**, 612 (1956).

[11] A. L. Ward, Physical review (1958), https://doi.org/10.1103/PhysRev.112.1852.

[12] A. L. Ward, Journal of Applied Physics **33**, 2789 (1962), https://doi.org/10.1063/1.1702550 .

[13] A. Fridman and L. A. Kennedy, *Plasma Physics and Engineering* (Taylor and Francis, New York, 2004).

[14] G. G. Gladush and A. A. Samokhin, J. Appl. Mech. Tech. Phys. **22**, 608 (1981).

[15] Yu. P. Raizer and S. T. Surgikov, Sov. Tech. Phys. Lett. **13**, 186 (1987).

[16] Yu. P. Raizer and S. T. Surgikov, High Temp. **26**, 304 (1988).

[17] J.-P. Boeuf, J. Appl. Phys. **63**, 1342 (1988).

[18] J. H. Ingold, Phys. Rev. A (1989).

[19] D. B. Graves and K. F. Jensen, IEEE Transactions on Plasma Science (1986).

[20] G. J. M. Hagelaar and L. C. Pitchford, Plasma Sources Sci. Technol. **14**, 722 (2005).

[21] V. I. Kolobov, J. Phys. D: Appl. Phys. **39**, R487 (2006).

[22] R. N. Franklin, *Plasma Phenomena in Gas Discharges* (Clarendon Press, Oxford, 1976).

[23] J. M. Dawson, Rev. Mod. Phys. (1983).

[24] J. P. Boeuf and E. Marode, J. Phys. D: Appl. Phy (1982).

[25] J. H. Miller and S. E. Page, *Complex Adaptive Systems - an introduction to computational models of social life* (Princeton university press, 2007).

[26] M. Mamei, R. Menezes, R. Tolksdorf, and F. Zambonelli, Journal of Systems Architecture **52**, 443 (2006), nature-Inspired Applications and Systems.

[27] Philosophical Transactions of the Royal Society B: Biological Sciences **237**, 37 (1952), http://rstb.royalsocietypublishing.org/content/237/641/37.full.pdf .

[28] D. Kondepudi and I. Prigogine, *Modern Thermodynamics Ű from Heat Engines to Dissipative Structures* (New York: John Wiley & Sons, 1998).

[29] V. Vanagand and E. Irving, Phys. Rev. Lett. (2001).

[30] G. Nicolis and I. Prigogine, *Self-Organization in Nonequilibrium Systems. From Dissipative Structures to Order through Fluctuations* (Wiley & Sons, New York, London, Sydney, Toronto, 1977).

[31] L. D. Landau and E. M. Lifshitz, *Statistical physics* (Pergamon International Library, 1969).

[32] L. V. Bertalanffy, *Modern theories of development*, edited by J. H. Woodger (Oxford University Press, 1933).

[33] E. Schrödinger, *What is life* (Cambridge University Press, 1944).

[34] H.-G. Purwins, H. U. Bödeker, and S. Amiranashvili, Adv. Physics **59**, 485 (2010).

[35] O. Lehmann, Annalen der Physik **4**, 1 (1902).

[36] P. Attard, arXiv.org (2012).

[37] L. Dabringhausen, O. Langenscheidt, S. Lichtenberg, M. Redwitz, and J. Mentel, J. Phys. D: Appl. Phys. **38**, 3128 (2005).

[38] M. S. Benilov and M. J. Faria, J. Phys. D: Appl. Phys. **40**, 5083 (2007).

[39] M. S. Benilov, J. Phys. D: Appl. Phys. **40**, 1376 (2007).

[40] M. S. Benilov and G. V. Naidis, J. Phys. D: Appl. Phys. **43**, 175204 (9pp) (2010).

[41] G. Iooss and D. D. Joseph, *Elementary Stability and Bifurcation Theory*, 2nd ed. (Springer, New York, 1990).

[42] P. G. C. Almeida, M. S. Benilov, and M. J. Faria, IEEE Trans. Plasma Sci. **39**, 2190 (2011).

[43] P. G. C. Almeida, M. S. Benilov, M. D. Cunha, and M. J. Faria, J. Phys. D: Appl. Phys. **42**, 194010 (21pp) (2009).

[44] J. D. Crawford, Rev. Mod. Phys. **63**, 991 (1991).

[45] D. Staack, B. Farouk, A. Gutsol, and A. Fridman, Plasma Sources Sci. Technol. **17**, 025013 (13pp) (2008).

[46] K. H. Schoenbach, M. Moselhy, and W. Shi, Plasma Sources Sci. Technol. **13**, 177 (2004).

[47] M. Moselhy and K. H. Schoenbach, J. Appl. Phys. **95**, 1642 (2004).

[48] N. Takano and K. H. Schoenbach, Plasma Sources Sci. Technol. **15**, S109 (2006).

[49] N. Takano and K. H. Schoenbach, in *Abstracts of the 2006 IEEE International Conference on Plasma Science* (IEEE, Traverse City, MI, USA, 2006) p. 247.

[50] B.-J. Lee, H. Rahaman, K. Frank, L. Mares, and D.-L. Biborosch, in *Proc. 28th ICPIG (Prague, July 2007)*, edited by J. Schmidt, M. Šimek, S. Pekárek, and V. Prukner (Institute of Plasma Physics AS CR, ISBN 978-80-87026-01-4, Prague, 2007) pp. 900–902.

[51] W. Zhu, N. Takano, K. H. Schoenbach, D. Guru, J. McLaren, J. Heberlein, R. May, and J. R. Cooper, J. Phys. D: Appl. Phys. **40**, 3896 (2007).

[52] B.-J. Lee, D.-L. Biborosch, K. Frank, and L. Mares, J. Optoelectron. Adv. Mater. **10**, 1972 (2008).

[53] W. Zhu, P. Niraula, P. G. C. Almeida, M. S. Benilov, and D. F. N. Santos, Plasma Sources Sci. Technol. **23**, 054012 (2014).

[54] W. Zhu and P. Niraula, Plasma Sources Sci. Technol. **23** (2014), the missing modes of self-organization in cathode boundary layer discharge in xenon, to appear in the Cluster Issue on Spots and Patterns.

[55] W. Zhu, P. Niraula, P. G. C. Almeida, M. S. Benilov, and D. F. N. Santos, Plasma Sources Science and Technology **23**, 054012 (2014).

[56] P. G. C. Almeida, M. S. Benilov, and M. J. Faria, Plasma Sources Sci. Technol. **19**, 025019 (13pp) (2010).

[57] P. G. C. Almeida and M. S. Benilov, Phys. Plasmas **20**, 101613 (2013).

[58] P. G. C. Almeida, M. S. Benilov, and D. F. N. Santos, ArXiv e-prints (2014), arXiv:1406.4394 .

[59] E. Hontañón, J. M. Palomares, X. Guo, R. Engeln, H. Nirschl, and F. E. Kruis, J. Phys. D: Appl. Phys. (2014).

[60] V. I. Arkhipenko, A. A. Kirillov, Y. A. Safronau, L. V. Simonchik, and S. M. Zgirouski, Plasma Sources Sci. Technol. (2009).

[61] H. Haken, *Synergetics, An Introduction*, Springer Series in Synergetics, Vol. 1 (Springer, Berlin, 1978).

[62] M. S. Benilov, Physica Scripta **58**, 383 (1998).

[63] M. S. Benilov, Plasma Sources Sci. Technol. **23**, 054019 (2014).

[64] M. S. Benilov, Sov. Phys. - Tech. Phys. **33**, 1267 (1988).

[65] G. M. J. Mackay, Physical Review Letters **15**, 309 (1920).

[66] C. H. Thomas and O. S. Duffendack, Phys. Rev. **35**, 72 (1930).

[67] S. M. Rubens and J. E. Henderson, Phys. Rev. **58**, 446 (1940).

[68] K. G. Emeleus, Int. J. Electronics **52**, 407 (1982).

[69] K. G. Mueller, Physical Review A **37**, 4836 (1988).

[70] Ch. Maszl, J. Laimer, and H. Störi, IEEE Trans. Plasma Sci. **39**, 2118 (2011).

[71] V. I. Arkhipenko, T. Callegari, Y. A. Safronau, L. V. Simonchik, and I. M. Tsuprik, Plasma Sources Sci. Technol. **22**, 045003 (2013).

[72] L. M. Ivan, G. Amarandei, M. Aflori, M. Mihai-Plugaru, C. Gaman, D. Dimitriu, C. Ionita, and R. W. Schrittwieser, acta physica slovaca **55**, 501 (2005).

[73] L. M. Ivan, G. Amarandei, M. Aflori, D. Dimitriu, and M. Sanduloviciu, IEEE Trans. Plasma Sci. **33**, 542 (2005).

[74] D. G. Dimitriu, M. Aflori, L. M. Ivan, C. Ionita, and R. W. Schrittwieser, Plasma Phys. Control. Fusion (2007).

[75] C. Charles, Plasma Sources Science and Technology **16**, R1 (2007).

[76] S. D. Baalrud, B. Longmier, and N. Hershkowitz, Plasma Sources Sci. Technol. **18**, 035002 (2009).

[77] S. Chauhan, M. Ranjan, M. Bandyopadhyay, and S. Mukherjee, Phys. Plasmas **23**, 013502 (2016).

[78] Y.-S. Park, Y. Lee, K.-J. Chung, and Y. seok Hwang, Rev. Sci. Instrum. **82**, 123303 (2011).

[79] R. S. Islamov, Phys. Rev. E **64**, 046405 (2001).

[80] Yu. Akishev, V. Karal'nik, I. Kochetov, A. Napartovich, and N. Trushkin, Plasma Sources Sci. Technol. (2014), high current cathode and anode spots in gas discharges at moderate and elevated pressures, to appear in the Cluster Issue on Spots and Patterns.

[81] Z. Chen, S. Zhang, I. Levchenko, I. I. Beilis, and M. Keidar, ARXIV (2017).

[82] R. S. Islamov and E. N. Gulamov, IEEE Trans. Plasma Sci. **26**, 7 (1998).

[83] M. S. Benilov, Plasma Sources Sci. Technol. **23** (2014).

[84] P. G. C. Almeida and M. S. Benilov, Phys. Plasmas **20** (2013).

[85] M. S. Bieniek, P. G. C. Almeida, and M. S. Benilov, Journal of Physics D: Applied Physics **49**, 105201 (2016).

[86] B. Scheiner, S. D. Baalrud, M. M. Hopkins, B. T. Yee, and E. V. Barnat, Physics of Plasmas **23**, 083510 (2016), https://doi.org/10.1063/1.4960382 .

[87] Z. Chen, S. Zhang, I. Levchenko, I. I. Beilis, and M. Keidar, Sci. Rep. **7**, 12163 (2017).

[88] M. S. Bieniek, P. G. C. Almeida, and M. S. Benilov, in *Proc. XXXIII ICPIG (9-14 July 2017, Estoril, Portugal)* (2017) p. 287.

[89] D. Mansuroglu, I. U. Uzun-Kaymak, and I. Rafatov, Phys. Plasmas **24**, 053503 (2017).

[90] Yu. P. Raizer and M. S. Mokrov, Phys. Plasmas **20**, 101604 (2013).

[91] I. Rafatov, Plasma Sources Sci. Technol. **25**, 065014 (2016).

[92] H.-G. Purwins and L. Stollenwerk, Plasma Phys. Control. Fusion **56**, 123001 (2014).

[93] J. P. Trelles, J. Phys. D: Appl. Phys. **49**, 393002 (2016).

[94] A. Bergner, M. Westermeier, C. Ruhrmann, P. Awakowicz, and J. Mentel, J. Phys. D: Appl. Phys. **44**, 505203 (2011).

[95] P. G. C. Almeida, M. S. Benilov, M. D. Cunha, and J. G. L. Gomes, Plasma Sources Sci. Technol. **22**, 012002 (2013).

[96] M. Schmidt, H. Schneidenbach, and M. Kettlitz, J. Phys. D: Appl. Phys. **46**, 435202 (2013).

[97] M. S. Benilov, J. Phys. D: Appl. Phys. **41**, 144001 (30pp) (2008).

[98] J. Mentel, J. Phys. D: Appl. Phys. **51**, 033002 (2018).

[99] M. S. Benilov, M. D. Cunha, and M. J. Faria, J. Phys. D: Appl. Phys. **42**, 145205 (17pp) (2009).

[100] R. Bötticher, W. Graser, and A. Kloss, J. Phys. D: Appl. Phys. **37**, 55 (2004).

[101] R. Bötticher and M. Kettlitz, J. Phys. D: Appl. Phys. **39**, 2715 (2006).

[102] P. G. C. Almeida, M. S. Benilov, and M. D. Cunha, J. Phys. D: Appl. Phys. **41**, 144004 (9pp) (2008).

[103] C. Wang, W. Li, X. Zhang, M. Liao, J. Zha, and W. Xia, IEEE Trans. Plasma Sci. **43**, 3716 (2015).

[104] M. S. Bieniek, P. G. C. Almeida, and M. S. Benilov, J. Phys. D: Appl. Phys. **49**, 105201 (2016).

[105] W. Zhu and N. Ike, private communication (2017).

[106] P. G. C. Almeida, M. S. Benilov, and M. J. Faria, J. Phys. D: Appl. Phys. **44**, 415203 (2011).

[107] V. N. Melekhin and N. Yu. Naumov, Sov. Phys. Tech. Phys. **29**, 888 (1984).

[108] A. V. Phelps, Z. Lj. Petrović, and B. M. Jelenković, Phys. Rev. E **47**, 2825 (1993).

[109] I. D. Kaganovich, M. A. Fedotov, and L. D. Tsendin, Tech. Phys. **39**, 241 (1994).

[110] Yu. D. Korolev and K. H. Schoenbach, in *Proc. XXVII ICPIG (Eindhoven, the Netherlands, July 2005)*, edited by E. M. van Veldhuizen (Eindhoven University of Technology, Eindhoven, 2005).

[111] M. S. Bieniek, P. G. C. Almeida, M. S. Benilov, W. Zhu, and P. Niraula, in *43rd IEEE Int. Conf. Plasma Sci. (ICOPS 2016)* (2016).

[112] W. Zhu and P. Niraula, private communication (2014).

[113] G. J. M. Hagelaar, F. J. de Hoog, and G. M. W. Kroesen, Phys. Rev. E **62**, 1452 (2000).

[114] A. Salabas, G. Gousset, and L. L. Alves, Plasma Sources Science and Technology **11**, 448 (2002).

[115] A. V. Azarov and V. N. Ochkin, J. Russ. Laser Res. **25**, 138 (2004).